Cooperative Intramolecular Dynamics Control the Chain-Length-Dependent Glass Transition in Polymers

Daniel L. Baker[ORCID],[1] Matthew Reynolds[ORCID],[1] Robin Masurel,[2] Peter D. Olmsted[ORCID],[2] and Johan Mattsson[ORCID][1,*]

[1]*School of Physics and Astronomy, University of Leeds, Leeds LS29JT, United Kingdom*
[2]*Department of Physics and Institute for Soft Matter Synthesis and Metrology,*
Georgetown University, Washington DC, 20057, USA

The glass transition is a long-standing unsolved problem in materials science. For polymers, our understanding of glass formation is particularly poor because of the added complexity of chain connectivity and flexibility; structural relaxation of polymers thus involves a complex interplay between intramolecular and intermolecular cooperativity. Here, we study how the glass-transition temperature T_g varies with molecular weight M for different polymer chemistries and chain flexibilities. We find that $T_g(M)$ is controlled by the average mass (or volume) per conformational degree of freedom and that a "local" molecular relaxation (involving a few conformers) controls the larger-scale cooperative α relaxation responsible for T_g. We propose that dynamic facilitation where a local relaxation facilitates adjacent relaxations, leading to hierarchical dynamics, can explain our observations, including logarithmic $T_g(M)$ dependences. Our study provides a new understanding of molecular relaxations and the glass transition in polymers, which paves the way for predictive design of polymers based on monomer-scale metrics.

Subject Areas: Materials Science, Soft Matter
Statistical Physics

I. INTRODUCTION

As a polymer melt is cooled, the timescale $\tau_\alpha(T)$ characterizing its structural (α) relaxation increases, eventually leading (in the absence of crystallization) to an arrested out-of-equilibrium amorphous solid called a glass [1]; since dynamic arrest depends on cooling rate [1], the glass-transition temperature is conventionally defined by choosing $\tau_\alpha(T_g) \equiv$ 100 s [2]. Variations in chain length and chain flexibility of polymers provide tremendous versatility, tunability, and processability. Thus, polymer glasses are ubiquitous, and they are found in construction materials (aerospace, medical implants, additive manufacturing), coatings, optical components, and membranes for controlled transport of ions, gases, or electrons. However, our fundamental lack of understanding of glass formation in polymers often restricts our ability to design materials with optimized performance.

Glass formation is often attributed to the reduced available "free" volume for molecular motion [3,4], the increasing elastic energy required to create this volume [5], or a decreasing configurational entropy [2,6]. The earliest theory for polymer glasses, due to Fox and Flory [7],

accounted for additional mobility in short-chain polymers due to the excess free volume around chain ends, leading to a smooth decrease in T_g for decreasing polymer molecular weight; a similar argument was later proposed in a lattice theory by Gibbs and DiMarzio [8] based on increasing configurational entropy near the chain ends. An alternative approach, based on excess free volume at chain ends, that could better account for short chain behaviour, was proposed by Ueberreiter and Kanig [9]. The more recent so-called generalized entropy theory is also a lattice model based on configurational entropy, originally designed for semiflexible polymers, which includes main- and side-chain bending energies [10], which also gives rise to a smooth decrease in $T_g(M)$ with decreasing M. A similar $T_g(M)$ behavior was also recently suggested based on the M-dependent nonaffine contributions to displacements induced upon deformation of a glass [11].

However, in 1975, Cowie [12], followed by others [13,14], demonstrated that polymers show a more complex $T_g(M)$ behavior, dividing into three separate regimes, roughly corresponding to an oligomeric short-chain ($\lesssim 2$ Kuhn steps), an intermediate ($\sim 2 - 10$ Kuhn steps), and a long-chain M-independent regime; clearly, a different approach is required to understand these observations.

A key difference between polymeric and nonpolymeric glass formers is the presence of polymer-specific intramolecular dihedral barriers, which are absent from the theories discussed above. Indeed, computer simulations suggest that the dynamic arrest mechanism (and thus T_g) of polymers is

significantly influenced by such barriers [15,16]. Moreover, in 1940, Kauzmann and Eyring [17] studied the viscosity of short-chain alkanes and inferred that viscous flow of polymers arises from a succession of elementary intramolecular movements within a "flow segment" with a typical characteristic size of about 5–10 bonds; this roughly corresponds to the size of the Kuhn "random walk" step size, which controls the equilibrium chain statistics [17–20]. Studies later attempted to link the α relaxation, and thus T_g, to faster relaxations on the scale of the flow segment [21–27], but there is still no consensus about this putative link.

The relative importance of intramolecular versus intermolecular relaxation dynamics in polymers has been inferred from high pressure experiments, which can separate the effects of temperature and volume [27–30]. The ratio $\mathcal{R}$ between the isochoric activation volume and isobaric activation enthalpy for the α relaxation in polymers is typically $\mathcal{R} \sim 0.4$–0.8, and a correlation between $\mathcal{R}$ and the monomer volume [28] has been identified. Note that $\mathcal{R} = 1$ implies that thermal energy, which regulates movements across intramolecular energy barriers and changes in cohesive energies, fully controls the dynamics, whereas $\mathcal{R} = 0$ implies that the dynamics are controlled solely by volume changes. For example, $\mathcal{R} = 0.73$ was found for poly(methyl methacrylate) (PMMA) [30] and $\mathcal{R} = 0.63$ for poly(styrene) (PS) [27]. Thus, both intermolecular and intramolecular motions play important roles in polymers, even though the balance between the two is system dependent, and intramolecular degrees of freedom (DOF) become increasingly important as the chain length grows.

Mode coupling theory (MCT) [31] successfully captures some phenomenology of both nonpolymeric [31,32] and polymeric [33,34] glass formers for $T \gg T_g$, but it fails near T_g, where thermal activation becomes important. Still, MCT-based analyses of experiments and simulations for $T \gg T_g$ suggest competing arrest mechanisms for polymers [15,33]. Schweizer and co-workers [35,36] went beyond MCT to incorporate activation barriers for both segmental "cage escape" and elastic deformation of the segment-surrounding matrix [5]. They treated the polymer melt as a fluid of effective Kuhn-sized hard spheres with multiple interaction sites, and based on this approach, they predicted a $T_g(M)$ smoothly growing with M [36]. However, this model lacks intramolecular barriers and the cooperativity necessitated by chain connectivity, and it relies on an unconventional assumption that properties of the Kuhn step depend on molecular weight. Thus, there is presently neither a satisfactory phenomenological understanding of $T_g(M)$ and its related relaxation dynamics nor any theory that incorporates intramolecular barriers, chain connectivity, and the necessary M-dependent variation of intermolecular and intramolecular dynamics.

Here, we present extensive experiments on the dependence of the glass-transition and associated dynamics on polymer chain length and chain flexibility, complemented by rotational isomeric state (RIS) simulations of chain dimensions. We propose a new framework for understanding the glass-transition dynamics of polymers based on cooperative

conformational rearrangements involving dihedral motion on a local (conformer) scale. For short chains, these rearrangements spread along the chain, resulting in a secondary (β) relaxation; for longer chains, chain folding divides the chain into Rouse-like β-relaxation "beads." The structural α relaxation (and thus T_g) results, in turn, from propagation of mobility through either intermolecular or intramolecular dynamic facilitation [37–40] of the β relaxations. The nature of this facilitated dynamic coupling varies with chain length, separating $T_g(M)$ into three distinct dynamic regimes, as originally proposed by Cowie [12].

II. RELAXATION DYNAMICS

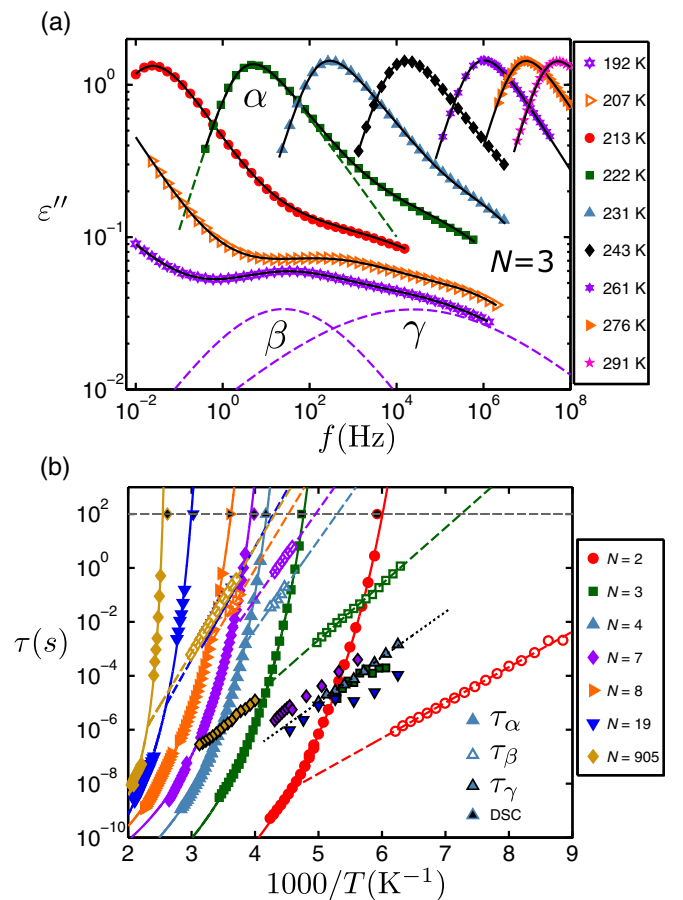We determine the molecular-weight (M)-dependent relaxation dynamics and T_g using broadband dielectric

FIG. 1. (a) Dielectric loss $\varepsilon''(f)$ for PMMA with $N = 3$ at different T. Dashed lines show α, β, and γ relaxations, while solid lines are fits to the spectra, as described in Appendix A. (b) Arrhenius plot showing the characteristic relaxation peak timescales: τ_α (filled symbols), τ_β (open symbols), and τ_γ (filled symbols, black outline) for PMMA with $N \in 2$–905. The solid lines are VFT fits to the τ_α data, the dashed lines are Arrhenius fits to $\tau_\beta(T)$, and the dotted line is an Arrhenius fit to $\tau_\gamma(T)$ for $N = 4$ (fits to other N are omitted for clarity). All fitting parameters are tabulated in Table VII. DSC data are shown as black-filled symbols at $\tau = 10^2$ s (horizontal dashed line), which defines T_g.

spectroscopy (BDS) and differential scanning calorimetry (DSC) (see Appendix A). The frequency-dependent dielectric loss $\varepsilon''(f)$ for oligomeric PMMA with a degree of polymerization $N = 3$ is shown in Fig. 1(a). We observe three distinct relaxation processes (loss peaks): α, β, and γ, where $\tau_\alpha > \tau_\beta > \tau_\gamma$. The α relaxation defines T_g, while the β and γ relaxations are typically assigned to molecular rearrangements that include both backbone and side-group rotations [22,23,41–43].

The peak relaxation times $\tau_p \equiv (2\pi f_p)^{-1}$ are plotted in Fig. 1(b) for PMMA with $N \in 2, \ldots, 905$. The α relaxation time follows the empirical Vogel-Fulcher-Tammann (VFT) expression $\tau_\alpha = \tau_0 \exp DT_0/(T - T_0)$ typically associated with glass formation [1,5]. Molecular relaxation times τ_β and τ_γ within the glassy nonequilibrium state, on the other hand

[Fig. 1(b)], typically follow simple Arrhenius behavior $\tau_i = \tau_{0i} \exp(\Delta H_i / RT)$, where ΔH is the activation enthalpy and R is the gas constant. The secondary relaxations are determined solely in the glassy state, where the analysis is straightforward and the behavior is Arrhenius. We determine $T_g(M)$ from the VFT fits by setting $\tau_\alpha(T_g) = 100$ s, and from DSC by determining the onset of the heat capacity step for a heating rate of 10 K min^{-1} (Appendix A).

III. T_g VARIATION WITH POLYMER CHAIN LENGTH AND CHAIN FLEXIBILITY

Traditionally, $T_g(M)$ for polymers is described using the Fox-Flory relation, $T_g^\infty - T_g \propto 1/M$, typically attributed to the dependence of free volume [7] or configurational
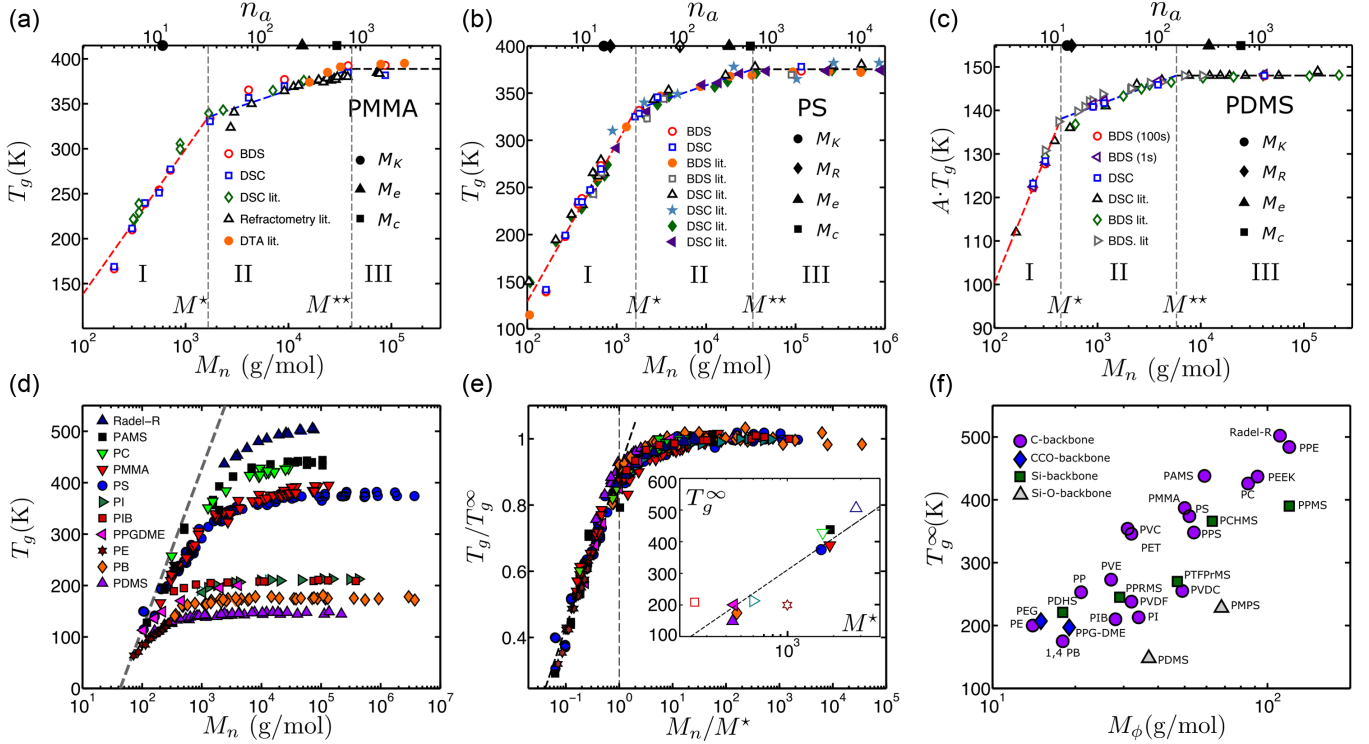

FIG. 2. (a)–(c) T_g as a function of the number-averaged molecular weight M_n and the number of backbone atoms n_a. We use M_n throughout except for Radel-R and one literature data set for PS (Appendix E), for which only the weight-averaged molecular weight M_w is known. Data from BDS and DSC are combined with literature data for PMMA, PS, and PDMS (Appendix E). The experimental values of $T_g(M)$ vary slightly because of the nature of the experimental probe, T_g definition, or polymer specification. For PDMS, these differences are more pronounced since T_g is only weakly varying with M ($\Delta T_g \sim 40$ K); a scaling factor $A \sim 1$–1.03 was thus introduced to collapse different PDMS data sets, where $A = 1$ for the T_g data from Ref. [47]. Since $T_g(M)$ for PDMS in Ref. [20] was defined for $\tau_\alpha = 1$ s, we plot our T_g data for PDMS both with the standard definition $\tau_\alpha = 100$ s ($A = 1.024$) and $\tau_\alpha = 1$ s ($A = 1.003$) to demonstrate that, except for an absolute shift in T_g, this yields the same shape of $T_g(M)$. The symbols on the upper abscissa denote the Kuhn molecular weight (filled black circle), the dynamical or Rouse molecular weight M_R (filled black diamond, or diamond for an alternative M_R definition [20]), the entanglement molecular weight M_e (filled black up-pointing triangle), and the critical molecular weight M_c (filled square); all values are tabulated in Table IV. The red, blue, and black dashed lines are fits, respectively, to $T_g = A_{I,II} + B_{I,II} \log_{10} M$ in regimes I and II, and $T_g = T_g^\infty$ in regime III. The vertical dashed lines at $M^\star$ and $M^{\star\star}$ denote the boundaries between the different regimes. (d) $T_g(M)$ for 11 different polymers (Appendix E) [48]. The dashed line indicates $T_g(M)$ for rigid nonpolymeric glass formers, as discussed in the text. (e) T_g/T_g^∞ vs $M/M^\star$, where $T_g^\infty \equiv T_g(M \to \infty)$. The inset shows T_g^∞ vs $\log_{10} M^\star$ (open symbols denote polymers with less certainty in $M^\star$ due to data that do not cover all three regimes). (f) T_g^∞ vs the mass M_ϕ per conformational degree of freedom for polymers with different backbone chemistries (Appendix E), as signified by different colors and shown in the legend.

entropy [8] on the number of chain ends (T_g^∞ is the long-chain limit of T_g). This relation often breaks down for oligomeric M [8,12,22,44–46]. Cowie *et al.* [12] demonstrated that $T_g(M)$ can be divided into three regimes separated by molecular weights $M^\star$ and $M^{\star\star}$, where

$$T_g \simeq A_{\text{I,II}} + B_{\text{I,II}} \log_{10} M \qquad (3.1)$$

in regimes I and II, and $T_g \simeq T_g^\infty$ in regime III. This behavior is demonstrated for PMMA, PS, and poly (dimethyl siloxane) (PDMS) in Figs. 2(a)–2(c).

PMMA and PS are relatively rigid polymers with carbon-based backbones and bulky side groups, whose T_g values vary significantly with M [$\Delta T_g > 200$ K for $N \in (2 - \infty)$]. In contrast, the Si-O backbone of PDMS is much more flexible [50] and has low rotational barriers [51], leading to a much smaller variation in $T_g(M)$ [$\Delta T_g < 40$ K for $N \in (2 - \infty)$; Fig. 2(c)]. Unlike PMMA and PS, PDMS can *also* be described by the Fox-Flory relation (Fig. 10), suggesting a less-pronounced regime behavior for more flexible polymers. To demonstrate the generality of these observations, $T_g(M)$ data for 11 polymers (Table III; Appendix E) are shown in Fig. 2(e) to collapse onto the scaling form $T_g/T_g^\infty = f(M/M^\star)$, where T_g^∞ and $M^\star$

(Appendix E) depend on chemistry [52]. We do not expect this mastercurve to be perfect, because of the weaker variation in T_g for flexible polymers; and because of the differences among various polymers in features such as local segmental packing, interactions (e.g., due to side groups), tacticity, and polydispersity. We find evidence for a linear relationship (on average) between T_g^∞ and $\log_{10} M^\star$ [inset to Fig. 2(e)] across all chemistries. Such a relationship implies that a single chemistry-dependent molecular weight controls the full $T_g(M)$ behavior of each polymer.

Characteristic molecular weights for polymers [black symbols on the upper abscissa of Figs. 2(a)–2(c)] include the Kuhn molecular weight M_K (which controls equilibrium flexibility) [53], the "dynamic" or Rouse bead molecular weight M_R (which controls unentangled polymer dynamics [20]), the entanglement molecular weight M_e, and the molecular weight M_c at which entanglements become active [50]; the characteristic molecular weights discussed in this work are summarized in Table I. It is apparent that none of these molecular weights consistently matches either $M^\star$ or $M^{\star\star}$.

Earlier studies [54–57] suggested a link between T_g^∞ and a metric based on the polymer's conformational DOF. Accordingly, we determine the molecular weight M_ϕ per DOF (Appendix E) and plot the relation $T_g^\infty(M_\phi)$ in Fig. 2(f)

TABLE I.   Characteristic molecular weights.

Molecular weight M	Type	Description
M_o	Monomer	Polymer repeat unit
M_ϕ	Conformer	M per conformational degree of freedom
M_w	Weight average	Weight-averaged molecular weight
M_n	Number average	Number-averaged molecular weight
M_K	Kuhn	M of a Kuhn step, defined by $L_c = N_K \ell_K$, $6R_g^2 = N_K \ell_K^2$, and mass $M = N_K M_K$, where N_K is the number of Kuhn steps of length ℓ_K and $M = M_K$ in a polymer of contour length L_c and total mass M. The experimental input is the polymer radius of gyration R_g^2; see Ref. [52].
M_R	Rouse (or dynamic bead size)	M of the shortest timescale and length-scale Rouse mode. It is typically determined as a parameter in fits of chain relaxation spectra to the Rouse model (e.g., from rheology, broadband dielectric spectroscopy, or quasielastic neutron scattering).
M_e	Entanglement	Mean M between entanglements
M_c	Critical	Minimum M at which entangled dynamics are observed; ($M_c > M_e$).
M_γ	γ relaxation	Characteristic M of the γ relaxation; the shortest length (or mass) scale relaxation relevant to the glass-transition dynamics, involving a few cooperative conformational rearrangements.
$M^\star$	β relaxation; chain folding	M that separates regime I from regime II, as defined from the $T_g(M)$ behavior; M below which the α relaxation (glass transition) has mixed intramolecular and intermolecular characteristics.
$M^{\star\star}$	Intramolecular to intermolecular α relaxation	M above which T_g is nearly constant; separates regime II from region III, as defined from the $T_g(M)$ behavior.

for polymers with backbone chemistries based on C (purple), C-C-O (blue), Si (green), and Si-O (silver). These data suggest a linear relation between T_g^∞ and $\log_{10} M_\phi$ for C-based backbones. A simple interpretation is that M_ϕ parametrizes the displaced volume incurred in conformational motion, so higher volume conformers correspond to higher T_g. Consistent with this, polymers with Si-based backbones have lower T_g^∞ for the same M_ϕ, which can be partially accounted for by the higher mass density of Si compared with C. For the Si-O-based polymers in Fig. 2(f) (PDMS and PMPS), the larger mass density of Si and O compared with C cannot account for the entire discrepancy. The greater flexibility of the Si-O backbone, lower dihedral barriers, oxygen-specific interaction energies, or the fact that larger backbone angles (143° vs 110°) incur larger

volumes during dihedral rotation could all contribute. For the 11 polymer chemistries of Figs. 2(d) and 2(e), we find $M^* \approx 24 M_\phi$ (Fig. 12), so $T_g(M)$ for polymers roughly follows $T_g(M) \simeq T_g^\infty(M_\phi) f(M/M_\phi)$, where $f(x)$ is a chemistry-independent function.

IV. CHAIN STRUCTURE AND CONFORMATIONS

The low-T equilibrium conformation of a single polymer chain has a regular sequence of dihedral angles. For example, low-T polyethylene (PE) is an all-trans (rodlike) molecule, whereas low-T isotactic PS is a rodlike helix with alternating trans and gauche conformations. At higher T, the activation of higher-energy dihedral sequences
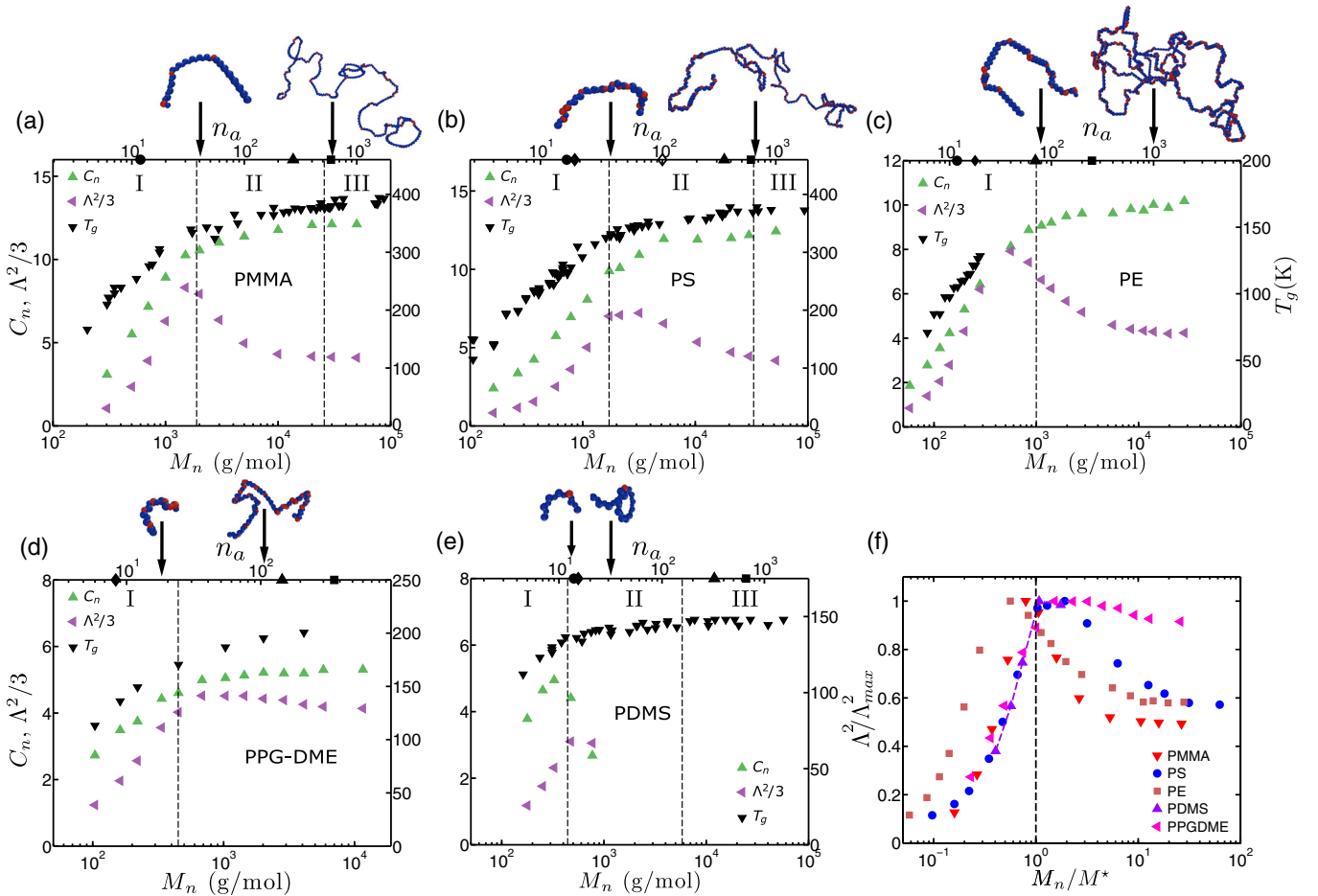

FIG. 3. (a)–(e) Glass-transition temperature T_g (inverted black triangles) from Fig. 2; the Flory characteristic ratio C_n (green triangles); and the aspect ratio $\Lambda^2 = \lambda_3^2/\lambda_1^2$, where λ_3^2 and λ_1^2 are, respectively, the largest and smallest eigenvalues of the average polymer conformational tensor (purple triangles) for (a) PMMA, (b) PS, (c) PE, (d) PPG-DME, and (e) PDMS. Here, C_n and Λ^2 are determined from RIS simulations performed at $T_g(M)$ for PMMA, PS, PPG-DME, or at $T_g = 200$ K for PE. The symbols on the top axes (filled black circle, filled black diamond, diamond, filled black triangle, filled black square) identify characteristic molecular weights as in Fig. 2. For each polymer chemistry, two typical molecular configurations are shown at the M indicated with arrows; here, bonds in excited dihedral states are shown in red. The dashed lines identify the crossovers between regimes I and II (at $M^\star$) and II and III (at $M^{\star\star}$). (f) $\Lambda^2/\Lambda_{\max}^2$ vs M/M^*, where all maxima $\Lambda_{\max}^2$ occur for $M \simeq M^\star$.

disorders the ground state so that longer polymers are more likely to be disordered and have the prolate ellipsoid shape of long, flexible, random coil polymers [58]; hence, polymers show M-dependent variations in average chain configurations and thus chain shapes [59].

To characterize the M-dependent variations in chain structure at $T = T_g(M)$, we use the RIS method [53] to calculate two metrics of chain structure [19]: (i) the Flory characteristic ratio $C_n = R_e^2/n_b l_b^2$, where R_e^2 is the average squared chain end-to-end distance, n_b is the number of backbone bonds, and l_b is the average bond length; and (ii) the aspect ratio $\Lambda^2 = \lambda_3^2/\lambda_1^2$ [19], where λ_3^2 and λ_1^2 are, respectively, the largest and smallest eigenvalues of the average polymer conformational tensor (Appendixes A and B). A small C_n denotes a more flexible molecule, while Λ^2 parametrizes the chain shape. Both metrics are calculated at $T_g(M)$ for PMMA, PS, PDMS, and poly(propylene glycol)-dimethyl ether (PPG-DME), or at $T_g = 200$ K for PE [48]. (Results for PE at different fixed T are shown in Appendix C; see Fig. 9.)

The M dependences of the two metrics and $T_g(M)$ are shown in Fig. 3; note that PPG-DME and PDMS are more flexible ($C_\infty = 5.1, 6.3$) than PMMA, PS, and PE ($C_\infty = 8.2, 9.6, 8.3$). Also, the low-energy state of PDMS comprises "loops" of $n_b \sim 24$ bonds [53,60], which are prohibited for long chains due to steric repulsion; hence, we limit our RIS calculations for PDMS to $n_b \lesssim 24$ [61]. We find that $C_n(M)$ for PMMA, PS, PE, and PPG-DME behaves similarly to $T_g(M)$ [20,36], while $C_n(M)$ for PDMS has a maximum because of loop formation [62].

All five polymers display a maximum [Fig. 3(f)] in Λ^2 near $M^\star$ (the maximum is less clear for the more flexible PPG-DME and PDMS; $M^\star$ for PE has a higher uncertainty, as discussed in Appendix C), which signifies a change in shape anisotropy, either due to the excited dihedral states leading to chain folding (PMMA, PS, PE, PPG-DME) or to loops in the ground state (PDMS), as can be seen by the characteristic chain configurations shown in Fig. 3. Hence, the change in dynamical character of $T_g(M)$ at $M^\star$ is manifested in structural changes near $M^\star$ [19]. Furthermore, the aspect ratio λ^2 approaches values characteristic of a Gaussian chain of approximately 11.9 [58], for $M \sim M^{\star\star}$, which also suggests a possible connection between $M^{\star\star}$ and equilibrium chain structure [52,64].

V. COMPARISON WITH $T_g(M)$ FOR NONPOLYMERIC GLASS FORMERS

For polymers, both chain length and local bulkiness (i.e., M_ϕ) control $T_g(M)$ [45,65]. To separate these two effects, we compare the polymer data to $T_g(M)$ for nonpolymeric, carbon-based, mainly aromatic, glass formers with as few conformers as possible; we denote these as "rigid" (we mainly use data from Ref. [66]; see Table VI). As shown in Fig. 4(a) (green circles), $T_g(M)$ for these nonpolymeric
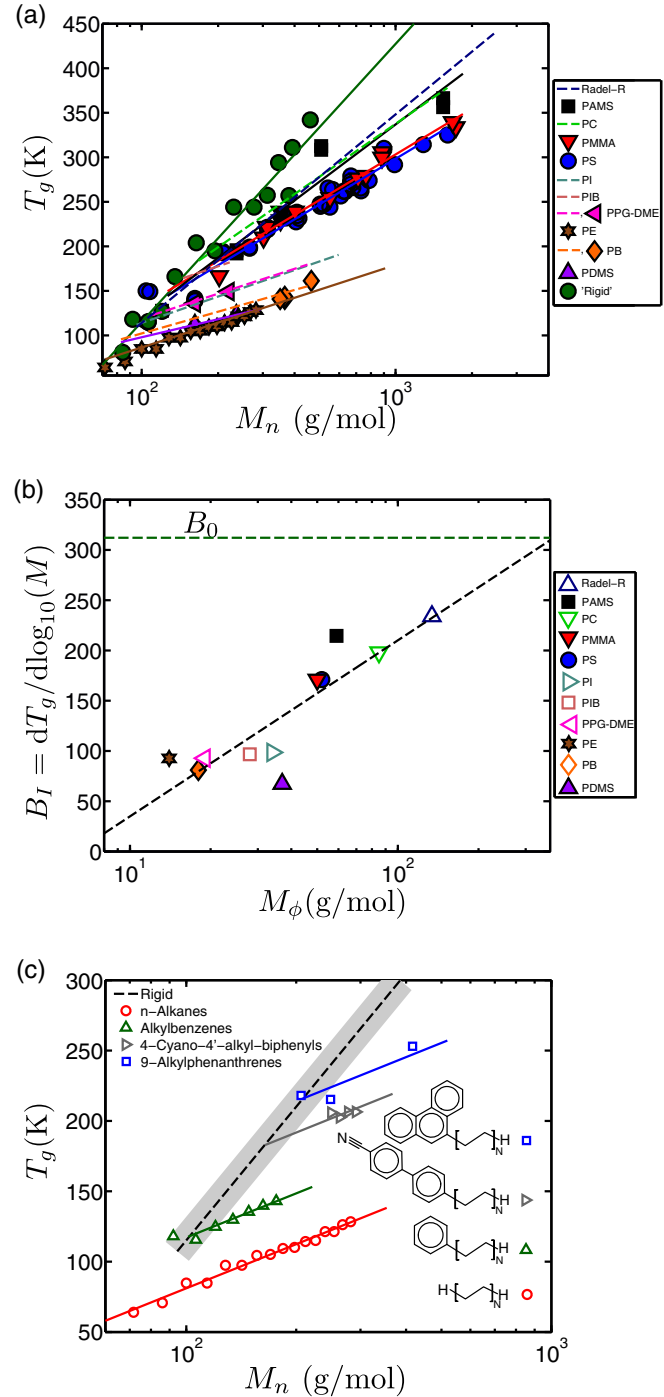

FIG. 4. (a) Glass-transition temperature T_g vs molecular weight M within regime I for polymers and rigid nonpolymeric molecules. The solid lines are fits of the form $T_g = A_I + B_I \log_{10} M$. For polymers with no (PC, PI, PIB, Radel-R) or sparse (PB, PPG-DME) data in regime I, the master curve in Fig. 2(e) is used to predict the regime I behavior, which is shown as dashed lines. (b) Chain mass sensitivity $B_I = dT_g/d\log_{10} M$ vs $\log_{10}(M_\phi)$; $B_0 = dT_g/d\log_{10} M$ for the nonpolymeric rigid molecules, shown as a horizontal dashed line. (c) T_g for four different chain series of n-alkanes (PE) with end groups of different size. The dashed shaded line marks the $T_g(M)$ behavior of the rigid nonpolymeric molecules, as shown by green circles in panel (a).

liquids is well described by $T_g(M) \simeq A_0 + B_0 \log_{10} M$, similarly to oligomeric glass formers in regime I. However, the chain mass sensitivity $B_I \equiv dT_g/d\log_{10} M$ for oligomers is smaller than B_0 for rigid molecules [green circles in Fig. 4(a)]. Moreover, B_I is typically smaller for more flexible oligomers [Fig. 4(b)], and it increases with M_ϕ. Thus, M_ϕ controls both B_I and the absolute value of T_g, consistent with the scaling of Fig. 2(e). Note that a semilogarithmic $T_g(M)$ form does not necessarily apply for any system of rigid molecules; see Appendix F for a detailed discussion. In contrast, a change in mass of one of the polymer end groups shifts the absolute value of T_g [67]. This is illustrated in Fig. 4(c), where n-alkanes (PE) are attached to end groups i with four different masses. Here, $T_g(M)$ of each series i can be described as $T_{g,i} = A_i + B \log_{10} M$, with B determined by the conformational character of the alkane chains (M_ϕ) and the intercept A_i increasing with the anchor group mass. Thus, separate control of the absolute T_g and the chain mass sensitivity B_I can be achieved by varying the mass (or volume) of an anchor end group.

VI. M-DEPENDENT ACTIVATION BARRIERS

The α relaxation of nonpolymeric glass formers near T_g involves correlated intermolecular motion on length scales of about 1–5 nm [68]. However, for polymers, $T_g(M)$ is strongly linked to the properties of the conformer [Figs. 2(e) and 2(f)], and the α relaxation has a significant intramolecular contribution due to chain connectivity and dihedral motion within the polymer backbone [15,16,21,22,69]. The β relaxation in polymers, in turn, has been interpreted as having a strongly intramolecular character, as demonstrated by its response to pressure [27,29]. Thus, we expect activation barriers for conformational relaxations to be of key importance for understanding glass-transition-related dynamics and T_g.

The activation enthalpies $\Delta H_{\beta,\gamma}$ for PMMA, determined from Arrhenius fits within the glassy state, are shown in Fig. 5(a). We find that

(i) ΔH_γ is roughly M independent;
(ii) $\Delta H_\beta \approx \Delta H_\gamma$ for $M \simeq M_\gamma$, suggesting that the β relaxation originates from more local γ relaxations acting on chain sections of mass $M_\gamma \simeq 200$ g/mol (4 backbone atoms or about 4 backbone conformers) [23];

(iii) ΔH_β increases with M for $M_\gamma < M < M^\star$ and is nearly M independent for $M \geq M^\star$, suggesting that the β relaxation in regimes II and III involves chain segments of size about $M^\star$.

For comparison, $\Delta H_{\beta,\gamma}$ for both PMMA and the more flexible polybutadiene (PB) are shown in Fig. 5(b), normalized by the average $\langle \Delta H_\gamma \rangle$ for each chemistry. For both polymers, the ratio $\Delta H_\beta/\langle \Delta H_\gamma \rangle \sim 2$–3 in regimes II and III, suggesting a degree of generality. Furthermore, the absolute values of $\Delta H_{\beta,\gamma}$ are lower for the more flexible PB (Appendix G; Fig. 16), consistent with the correlation between the conformational dihedral barrier height and T_g observed in simulations [15]. The general nature of the observed $\Delta H_\beta(M)$ behavior is similar to $\Delta H_\beta(M)$ of PS, PAMS, PC, and PDMS estimated from calorimetry experiments at varying heating rates following a temperature quench and subsequent glassy aging [22,76].

To investigate how the α relaxation (and thus T_g) relates to the β and γ relaxations, we determine the activation enthalpy $\Delta H_\alpha(M)$ for the α relaxation at T_g in two different ways, and we obtain consistent results [77]. The $\Delta H_\alpha(M)$ data shown in open triangles in Fig. 5(a) are determined from $\tau_\alpha(T_g) = \tau_0 \exp[\Delta H_\alpha(T_g)/RT_g]$ by setting $\tau_0 = \tau_0^{\text{micr}} = 10^{-12}$ s, where τ_0^{micr} is a microscopic timescale. The data shown in filled triangles are instead determined by equating $\tau_\alpha(T_g)$ from the Arrhenius relation above to $\tau_\alpha(T_g) = \tau_0 \exp[(DT_0/(T_g - T_0)]$ [where τ_0, D, and T_0 are VFT fitting parameters—see Fig. 1(b) —which yields $\Delta H_\alpha \equiv DT_0 RT_g/(T_g - T_0)$] [78].

As shown in Fig. 5(a), we find that $\Delta H_\alpha \approx \Delta H_\beta$ for $M \lesssim M^\star$, suggesting a similar nature of the two relaxations near $M^\star$. This result suggests that intramolecular rearrangements on the scale of $M^\star$ control the α relaxation for $M > M^\star$, where the chains are "folded," as shown in Fig. 3 [19]. Moreover, the complex M-dependent interrelationship between $\Delta H_\alpha(M)$ and $\Delta H_\beta(M)$ identified here for polymers [see Fig. 5(a)] strongly contrasts with the behavior observed in nonpolymeric glass formers, where a fixed M-independent ratio of $\Delta H_\alpha/\Delta H_\beta$ is typically observed [79]. Importantly, the activation enthalpies ΔH_α (regimes I and II) and ΔH_β (regimes I) appear to depend logarithmically on M for oligomeric and intermediate M chains, as shown in Fig. 5(a). A similar logarithmic M dependence has also been observed for the activation enthalpy of the high-T viscosity $\Delta H_\eta(M)$ in both experiments and computer simulations [18,19].
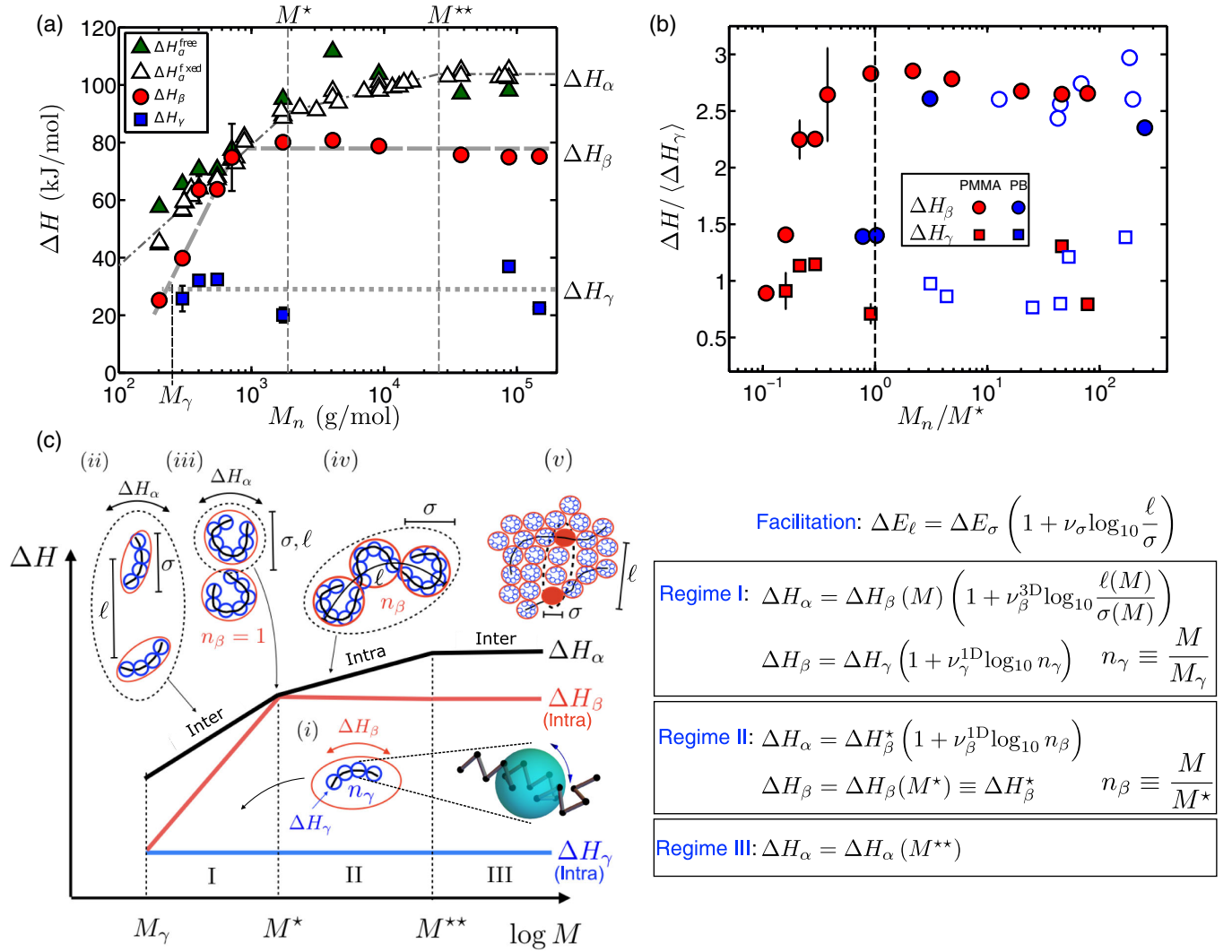
FIG. 5. (a) Activation enthalpies $\Delta H_{\alpha,\beta,\gamma}(M)$ for PMMA. Note that $\Delta H_\alpha(M)$ data were determined from $T_g(M)$ using a fixed $\tau_0 = 10^{-12}$ s (open triangles) or from the VFT fits in Fig. 1(b), as discussed in the text (filled triangles). Here, M_γ, $M^\star$, and $M^{\star\star}$ (described in the text) are marked as vertical dashed lines. The horizontal lines signify the average values of ΔH_γ (dotted, $M > M_\gamma$), ΔH_β (dashed, $M > M^*$), and ΔH_α (dot-dashed, $M > M^{\star\star}$). (b) $\Delta H_{\beta,\gamma}(M/M^\star)$ for PMMA and PB, normalized by their respective averages $\langle\Delta H_\gamma\rangle$; PB data from the literature [70–75] are shown as open symbols. Error bars in panels (a) and (b) represent the standard deviations obtained through least-mean-squares fitting of the secondary relaxation time data shown in Fig. 1(b). (c) Sketch of the activation enthalpy behavior for $\Delta H_{\alpha,\beta,\gamma}(M)$ for polymers. The equations describe the activation enthalpies due to facilitation in the different regimes, and the five cartoons (i)–(v) are described in detail in the text.

VII. DYNAMIC FACILITATION

Logarithmic activation barriers are a hallmark of hierarchical relaxations, and they are observed in dynamic facilitation models, in which spatially asymmetric kinetic constraints control relaxation [37,38]. A simple example is the one-dimensional East model [38,39,80], which describes a chain of "spins" (or "relaxation beads" in terminology appropriate for polymer relaxations) where each spin (or relaxation bead) can relax only when its neighbor on one side has relaxed. This simple asymmetric kinetic constraint gives rise to cooperative hierarchical dynamics and the main characteristics of glass-formation,

including dynamic heterogeneities and a broad distribution of relaxation times [80]. In this class of models, which have been successfully applied to intermolecular (3D) relaxation dynamics in nonpolymeric glass formers [80], relaxation on a length scale $\ell(T)$ separating mobile spins (relaxation beads) of size σ requires an activation barrier $\Delta E_\ell = \Delta E_\sigma[1 + \nu \log_{10}(\ell/\sigma)]$, where ΔE_σ is the barrier for a spin flip (bead relaxation). The factor $\nu \sim \mathcal{O}(1)$ has been determined for several different models, and it represents the nature and number of pathways available for facilitation [37,80,81]. For the East model of a one-dimensional spin chain, $0.72 < \nu < 1.4$ [81]; $\nu \simeq 0.25$ was estimated for several small-molecule glass formers based

on modeling calorimetry data [80]; and $\nu \simeq 0.35$–0.62 was determined for simulated 2D and 3D glass formers using several different interaction potentials [37].

If we apply this picture to cooperative intramolecular (1D) relaxation in polymers, then the activation barrier for relaxing a strand of n_{bead} beads is given by $\Delta E_{\text{strand}} = \Delta E_{\text{bead}}(1 + \nu_{\text{bead}}^{1D} \log_{10} n_{\text{bead}})$, where ΔE_{bead} is the barrier for relaxing a single bead [38,80], Here, a "bead" constitutes the part of the chain that undergoes cooperative rearrangements. The similarity [see Fig. 5(a)] between the β- and γ-relaxation behavior within regime I [$\Delta H_\beta = \Delta H_\gamma(1 + \nu_\gamma^{1D} \log_{10} n_\gamma)$] and the α- and β-relaxation behavior within regime II [$\Delta H_\alpha = \Delta H_\beta(1 + \nu_\beta^{1D} \log_{10} n_\beta)$] suggests that similar physical descriptions might be adopted in both cases. Hence, the nearly M-independent β relaxation in regime II plays a role similar to that of the nearly M-independent γ relaxation within regime I, where $n_\gamma \equiv M/M_\gamma$ and $n_\beta \equiv M/M_\beta$ are the numbers of relaxation beads per chain in either regime, and the parameters ν_γ^{1D} and ν_β^{1D} characterize the facilitation kinetics, which depend on both the material and the facilitation mechanism (our data suggest $\nu_\gamma^{1D} \simeq 2.0$ and $\nu_\beta^{1D} \simeq 0.16$).

In regimes I and III, the α relaxation is controlled by intermolecular (3D) facilitation between β-relaxation beads, and $\Delta H_\alpha = \Delta H_\beta[1 + \nu_\beta^{3D} \log_{10}(\ell/\sigma)]$, where ℓ is the average distance between β-relaxation beads of size σ; in contrast, within regime II, the α relaxation is controlled by intramolecular (1D) facilitation between β-relaxation beads [82].

We propose the following scenario for the observed hierarchy, as illustrated in Fig. 5(c). In regime I, intramolecular dynamic facilitation between γ-relaxation beads, governed by intramolecular barriers, induces the β relaxation [sketch (i); Fig. 5(c)], while the α relaxation arises from intermolecular facilitated dynamics, on a length scale $\ell(T)$ set by the average distance between β relaxations of size σ that increase with M [Fig. 5(c)(ii)]. The semilogarithmic M dependence of T_g and thus ΔH_α in regime I follows from the $\log_{10} M$ dependence of ΔH_β modulated by the M dependence $\ell(M)/\sigma(M)$. The ratio ℓ/σ decreases with M, and for $M \sim M^\star$, the data suggest $\ell \approx \sigma$, leading to effectively intramolecular dynamics where $\Delta H_\alpha \approx \Delta H_\beta$ [Fig. 5(c)(iii)]. Subsequently, within regime II, the α relaxation arises from intramolecular dynamic facilitation between β beads [Fig. 5(c)(iv)], each with an essentially fixed size of about $M^\star$ and activation barrier $\Delta H_\beta^\star$ [87].

For long enough chains, the intramolecular α relaxation mechanism becomes kinetically unfavorable (at $M^{\star\star}$), so within regime III, the α relaxation occurs through effectively intermolecular facilitation between the β beads, akin to the α relaxation within regime I [Fig. 5(c)(v)]. There is no general link between $M^{\star\star}$ and the onset of entanglements at M_c for polymers [64]. However, for polymers with significant side chains and thus large packing lengths [90] such as PMMA and PS (Table IV, Fig. 12), we speculate

that the onset of entanglements is likely to hinder the intramolecular α-relaxation dynamics of regime II; such an effect would be consistent with the observations that $M^{\star\star} \approx M_c$ for PMMA and PS, as shown in Figs. 2(a) and 2(b). We also note that $M^{\star\star}$ could be related to the onset of Gaussian chain statistics, as shown in Fig. 3.

VIII. CONCLUSION AND OUTLOOK

In this work, we have mapped out the relaxation dynamics and chain conformational structure, as a function of chain length, for polymers characterized by different chain flexibilities and local packing properties. We show that the molecular weight (M)-dependent glass-transition temperature $T_g(M)$ for polymers can be collapsed onto a master curve using a *single* chemistry-dependent parameter, which balances local conformational dynamics with packing. We find that the average molecular weight or volume per conformational degree of freedom, the conformer, is a relevant choice for this parameter. Moreover, a chain-length-dependent interplay between intermolecular and intramolecular relaxation dynamics results in a delineation of $T_g(M)$ into three characteristic dynamic regimes, where two of these are well characterized by a logarithmic M dependence. We find that the structural α relaxation, and thus T_g, is linked to more local secondary β and γ relaxations according to a hierarchical scheme, where the γ relaxation, involving a few conformers, acts as a fundamental excitation. Finally, we demonstrate that dynamic facilitation can explain both the relation between the molecular α, β, and γ relaxations observed in polymers, and the observed logarithmic $T_g(M)$ behaviors, as a direct result of hierarchical relaxation dynamics arising naturally due to dynamic facilitation.

The facilitation picture we propose suggests a new paradigm that couples local cooperative intramolecular motions on the scale of a few bonds to longer length-scale intramolecular and/or intermolecular motions, in turn resulting in structural relaxation. We suggest that facilitation can occur *along* the chain, as well as between chains, because of the cooperativity necessitated by substantial intramolecular barriers. Each form of facilitation can be expected to have different character and parameters (such as the facilitation exponent ν), which depend on the details of the cooperative pathways available for the relaxation [91]. We note, however, that we do not expect prominent intramolecular facilitation in flexible polymers for which the activation barriers for main-chain bond reorientations are about $\mathcal{O}(k_B T)$, thus enabling smooth reorientation. Moreover, our study has been limited to a relatively simple class of polymers; systematic variation of side groups, inclusion of more complex backbones (such as conjugated polymers), or copolymerization form natural extensions to this work. Importantly, our results could pave the way for efficient predictive design of polymers based solely on the monomer structure that controls the dynamics on the conformer length scale.

The data in this paper are available in the Leeds Data Repository [92].

APPENDIX A: METHODS

1. Broadband dielectric spectroscopy

BDS measurements were performed to determine the complex permittivity, $\varepsilon^*(f) = \varepsilon'(f) - i\varepsilon''(f)$ over a frequency range of $10^{-2} \leq f \leq 10^6$ Hz using a Novocontrol Alpha-A dielectric analyzer, and over a frequency range of $10^6 \leq f \leq 10^9$ Hz using an Agilent 4219B RF Impedance analyzer. For the lower frequency range, the samples were measured between two circular electrodes (20 or 40 mm diameter) with a spacing of 100–200 μm, and for the higher frequency range between two circular electrodes (10 mm diameter) with a spacing of 100 μm. The temperature was controlled using a Novocontrol Quatro system with an accuracy of 0.1 K. The complex permittivity measured at a particular temperature was analyzed using a sum of contributions from molecular relaxations as well as a contribution to the dielectric loss ε'' from ionic dc conductivity (σ_{dc}) when observed within the experimental window, $\varepsilon^* = -i\sigma_{dc}/(2\pi f \varepsilon_0)$. Each relaxation contribution was described using the Havriliak-Negami (HN) expression [42],

$$\varepsilon^* = \varepsilon_\infty + \frac{\Delta\varepsilon}{(1 + (i2\pi f \tau_{HN})^m)^n}, \qquad \text{(A1)}$$

where $\Delta\varepsilon$ is the dielectric strength, ε_∞ is the high-frequency permittivity, and τ_{HN} is a characteristic relaxation timescale. The parameters m and n describe the shape of the relaxation response; m and mn are the power-law exponents of the low- and high-frequency sides of the loss peak, respectively. The β and γ relaxations were generally well described using symmetrically stretched (Cole-Cole) loss peaks ($n = 1$) for which the loss-peak relaxation time was $\tau_p = \tau_{HN}$. The α-relaxation loss peaks, as well as the β relaxation for the highest M PMMA, on the other hand, were asymmetrically stretched, and τ_p was instead obtained from τ_{HN}, m, and n using a previously derived expression [42].

2. Differential scanning calorimetry

DSC measurements were performed using a TA instruments Q2000 heat flux calorimeter, with a liquid nitrogen cooling system for the temperature control. The polymer samples (weight of about 10 mg) were prepared in hermetically sealed aluminium pans, and measurements of the specific heat capacity as a function of temperature were performed for heating/cooling rates of 10 K/ min. The glass transition was manifested as a step in the specific heat capacity, and the reported T_g values were determined on heating from the onset temperatures corresponding to the steps.

APPENDIX B: ROTATIONAL ISOMERIC STATE FORMALISM AND CALCULATIONS

Flory's RIS theory [53] is used to calculate conformational chain properties such as the average end-to-end distance R_e, the gyration radius R_g, and the gyration tensor **Q**. Polymer chains comprise n_a backbone atoms, $n_b = n_a - 1$ backbone bonds, and $n_d = n_a - 3$ dihedral angles. Polymer backbone bonds typically have one, two, or three accessible dihedral angles ϕ_i per monomer; each ϕ_i is assumed to have discrete dihedral states. For example, in PE, the nomenclature "trans" commonly denotes a dihedral angle of $\phi = 180°$, leading to a planar zigzag backbone for the ground-state structure, while "gauche" refers to $\phi = \pm 60°$, which leads to a nonplanar backbone (a different convention for the dihedral angle is sometimes used, where trans refers to $\phi = 0°$ and gauche to $\phi = \pm 120°$). The conditional probability that a dihedral angle ϕ_i is followed by an angle ϕ_{i+1} is proportional to the matrix element $U_{\phi_i,\phi_{i+1}}$ of a so-called transfer matrix **U** [53], which is a square matrix with rank given by the number of dihedral angles for a given bond. By using this matrix, the probability $\mathcal{P}$ of finding an entire sequence of dihedral states $\Phi = \{\phi_1, \phi_2, \ldots, \phi_{N_d}\}$ can be calculated as the joint probability of finding ϕ_1 next to ϕ_2, ϕ_2 next to ϕ_3, and so on:

$$\mathcal{P}_{\{\Phi\}} = \frac{1}{\mathcal{Z}} U^*_{1,\phi_1} \prod_{i=1}^{n_d-1} U_{\phi_i,\phi_{i+1}}, \qquad \text{(B1)}$$

$$\mathcal{Z} = \boldsymbol{q}_0 \cdot \mathbf{U}^* \cdot \mathbf{U}^{n_d-1} \cdot \boldsymbol{q}_1, \qquad \text{(B2)}$$

$$\boldsymbol{q}_0 = (1, 0, \ldots), \qquad \boldsymbol{q}_1 = (1, \ldots 1), \qquad \text{(B3)}$$

where $\mathcal{Z}$ is the partition function, $\mathbf{U}^*$ is the transfer matrix for the first dihedral angle, the vector $\boldsymbol{q}_0$ defines the plane of the initial two bonds to be the trans plane, and the vector $\boldsymbol{q}_1$ ensures that all states are counted. The first two bonds of the chain define the initial plane from which subsequent bonds are accessed via the dihedral angles and bond angles for the specific polymer.

For polymers with multiple distinct dihedral angles per monomer, this can be generalized using different transfer matrices **U** for each dihedral in the monomer; for a polymer such as PDMS, one finds (see Fig. 6)

$$\mathcal{Z} = \boldsymbol{q}_0 \mathbf{U}^* \cdot (\mathbf{U}_b \mathbf{U}_a)^{N-1} \cdot \boldsymbol{q}_1, \qquad \text{(B4)}$$

where N is the number of monomers in the chain (degree of polymerization).

The RIS method ignores interactions along the chain of longer range than those between adjacent dihedral angles. Thus, very large side groups or charged polymers are poorly described, as are excluded volume effects resulting from distant monomers, which is generally a good approximation because of the screening of excluded volume in melts [93]. A notable exception encountered here is the ground-state configuration of PDMS, which involves a loop of about 24 bonds (12 monomers) in size, which will overlap in the ground state. As described in the main text, at temperatures near T_g for low M, these loops are not strongly disordered by excited gauche states [53,60].

Monte Carlo (MC) simulations are performed to sample the RIS distribution of dihedral angles along the chain. A MC step controls the transitions between rotational isomeric states Φ. Each Monte Carlo step corresponds to flipping a randomly chosen dihedral angle to a different dihedral angle, $\phi_i \to \phi_i'$ (e.g., from trans to gauche). The new dihedral conformation is then accepted or rejected using the Metropolis algorithm, with probabilities given by Eq. (B1). We typically perform 100 000 MC attempts in order to equilibrate a molecule at a given temperature, and conformational averages are calculated using the next 200 000 steps. Since we use $n_d \simeq 1$–2000 dihedral angles, the entire polymer is sampled from 100 to 200 000 times during the equilibration stage, depending on n_d and thus the polymer length.

The spatial position $\boldsymbol{r}_i$ of backbone atom i is given by

$$\boldsymbol{r}_i = \boldsymbol{r}_1 + \sum_{j=1}^{i-1} \boldsymbol{b}_j, \qquad (\text{B5})$$

where $\boldsymbol{r}_1$ is the first atom, and bonds are transformed along the chain by

$$\boldsymbol{b}_i = b_i \mathbf{T}_i \cdot \hat{\boldsymbol{b}}_{i-1}, \qquad (\text{B6})$$

for $i > 2$, where b_i is the bond length, $\hat{b}$ is a unit bond vector, and the bond transformation matrix is given by

$$\mathbf{T}_i = \begin{pmatrix} \cos\theta_i & \sin\theta_i & 0 \\ \sin\theta_i \cos\phi_i & -\cos\theta_i \cos\phi_i & \sin\phi_i \\ \sin\theta_i \cos\phi_i & -\cos\theta_i \sin\phi_i & -\cos\phi_i \end{pmatrix}, \qquad (\text{B7})$$

where θ_i is the bond angle and ϕ_i is the dihedral angle.

We study polymers whose repeat unit comprises two bonds (PS, PI, PDMS, etc.), a single bond (PE), or three bonds (PPG-DME). Each distinct bond in a repeat unit has a bond length, a bond angle, and a set of dihedral angles. The polymers PMMA, PS, and PPG-DME are stereoisomeric polymers and thus have tacticity, i.e., asymmetric side groups that lead to local chiral symmetry (right- or left-handedness) depending on the sequence of side groups (Fig. 6). We study atactic polymers, which correspond to a disordered mixture of chirality along the chain due to random right or left positions of the side groups. This tacticity can be quantified by either (i) the fraction of meso (two successive side groups in the same position) or racemic (two successive side groups in opposite positions) diads in polymers with a single atom between side groups (PMMA, PS); or (ii) the total proportion of right-handed side groups in polymers separated by two atoms (PPG-DME). In the latter
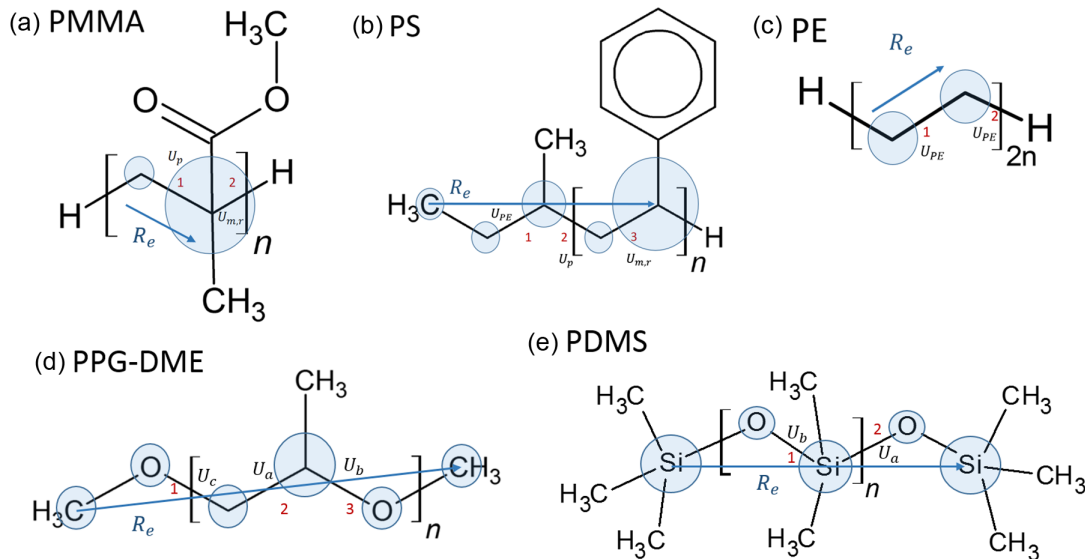

FIG. 6. Polymer structures used in the RIS calculations. The end-to-end vectors $\boldsymbol{R}_e$ are marked with blue arrows, red numbers label bonds about which dihedral angles rotate, and blue circles show the atoms used to calculate the gyration tensor, with a spherical volume equal to the volume of all included atoms. The number of monomers is n. The volume of the backbone atom and its side groups is assumed to be localized on the backbone atom. For example, the blue circle centered on the Si atoms at the ends of PDMS represents the volume of Si and three CH_3 groups, while interior volumes comprise a Si and two CH_3 groups.

TABLE II. RIS data used for calculations. The transfer matrices **U** describe the relative weights of successive rotational isomeric states specified by the dihedral angles. The matrix indices label (t, g) or (t, g^+, g^-) dihedral angles. Matrix elements have the form $\sigma = \Gamma_\sigma e^{-H_\sigma/k_B T}$, $\omega = \Gamma_\omega e^{-H_\omega/k_B T}$, ... PE has a single, unique bond, specified by **U**, and is calculated at five different temperatures: 70, 110, 148, 200, and 237 K. All other polymers are calculated at $T_g(M)$ based on data as follows: PDMS, Ref. [12]; PMMA, experimental data from Fig. 2 of main text; PPG-DME, interpolated from experimental data in Fig. 2; PS, experimental data from Fig. 2. PDMS has two distinct bonds (Fig. 6) specified by $\mathbf{U}_a$ and $\mathbf{U}_b$. PS has two distinct bonds, the first specified by $\mathbf{U}_p$ and the second with a phenyl ring asymmetrically placed on either the right or left side relative to the chain direction. Similarly, PMMA has two distinct bonds and an asymmetric carbon. In each case, $\mathbf{U}_m$ specifies the meso diad (two successive right or left asymmetric carbons), and $\mathbf{U}_r$ specifies the racemic diad (right/left or left/right sequence). PPG-DME has three dihedral angles (a, b, c) and one asymmetric carbon on the backbone chain per repeat unit. Matrices corresponding to a left (S) asymmetrical carbon are obtained from the right (R) matrices according to $\mathbf{U}_i^S = \mathbf{P}\mathbf{U}_i^R\mathbf{P}$.

Polymer	Transfer Matrices	Enthalpies kJ/mol	Bond lengths and angles	Dihedral angles	T_{cal} K	Ref.
PE	$\mathbf{U} = \begin{pmatrix} 1 & \sigma & \sigma \\ 1 & \sigma & \sigma\omega \\ 1 & \sigma\omega & \sigma \end{pmatrix}$	$\begin{array}{ccc} & H & \Gamma \\ \hline \sigma & 2.1 & 1 \\ \omega & 8.6 & 1 \end{array}$	C-C = 153 pm C-C-C = 112°	$t = 180°$ $g^+ = +60°$ $g^- = -60°$	433	[88]
PDMS	$\mathbf{U}_a = \begin{pmatrix} 1 & \sigma & \sigma \\ 1 & \sigma' & 0 \\ 1 & 0 & \sigma' \end{pmatrix}$ $\mathbf{U}_b = \begin{pmatrix} 1 & \sigma & \sigma \\ 1 & \sigma' & \delta \\ 1 & \delta & \sigma' \end{pmatrix}$	$\begin{array}{ccc} & H & \Gamma \\ \hline \sigma & 3.6 & 1 \\ \sigma' & 3.6 & 1 \\ \delta & 8.0 & 1 \end{array}$	Si-O = 164 pm O-Si-O = 110° Si-O-Si = 143°	$t = 180°$ $g^+ = +60°$ $g^- = -60°$	343	[89]
PS	$\mathbf{U}_p = \begin{pmatrix} 1 & 1 \\ 1 & 0 \end{pmatrix}$ $\mathbf{U}_m = \begin{pmatrix} \omega'' & 1/\eta \\ 1/\eta & \omega/\eta^2 \end{pmatrix}$ $\mathbf{U}_r = \begin{pmatrix} 1 & \omega'/\eta \\ \omega'/\eta & 1/\eta^2 \end{pmatrix}$	$\begin{array}{ccc} & H & \Gamma \\ \hline \eta & -1.7 & 0.8 \\ \omega & 8.3 & 1.3 \\ \omega' & 8.3 & 1.3 \\ \omega'' & 9.2 & 1.8 \end{array}$	C-C = 153 pm C-C$^\alpha$-C = 112° C$^\alpha$-C-C$^\alpha$ = 114°	$t = 175°$ $g = +60°$ (meso) $g = -60°$ (racemic)	300	[90]
PMMA	$\mathbf{U}_p = \begin{pmatrix} 1 & 1 \\ 1 & 0 \end{pmatrix}$ $\mathbf{U}_m = \begin{pmatrix} 1 & \alpha \\ \alpha & \alpha^2/\beta \end{pmatrix}$ $\mathbf{U}_r = \begin{pmatrix} \beta & \alpha \\ \alpha & \alpha^2/\beta \end{pmatrix}$	$\begin{array}{ccc} & H & \Gamma \\ \hline \alpha & 4.6 & 1.6 \\ \beta & -2.5 & 1.4 \end{array}$	C-C = 153 pm C-C$^\alpha$-C = 110° C$^\alpha$-C-C$^\alpha$ = 122°	$t = 180°$ $g = +60°$ (meso) $g = -60°$ (racemic)	300	[91]
PPG-DME	$\mathbf{U}_a^R = \begin{pmatrix} 1 & \alpha & \beta \\ 1 & \alpha & \beta\omega \\ 1 & \alpha\omega & 0 \end{pmatrix}$ $\mathbf{U}_b^R = \begin{pmatrix} 1 & 0 & 1 \\ 1 & 0 & \omega \\ 1 & 0 & 1 \end{pmatrix}$ $\mathbf{U}_c^R = \begin{pmatrix} 1 & \sigma & 0 \\ 1 & 0 & 0 \\ 1 & 0 & \sigma \end{pmatrix}$ $\mathbf{P} = \begin{pmatrix} 1 & 0 & 0 \\ 0 & 0 & 1 \\ 0 & 1 & 0 \end{pmatrix}$	$\begin{array}{ccc} & H & \Gamma \\ \hline \alpha & -1.26 & 1 \\ \beta & 1.46 & 1 \\ \sigma & 5.4 & 1 \\ \omega & 1.7 & 1 \end{array}$	C-C = 153 pm C-O = 143 pm C-O-C = 111.5° C-C-O = 110°	C-C: $t = 180°$, $g = 60°$ C-O: $t = -160°$, $g^+ = 60°$, $g^- = -80°$ O-C: $t = 180°$, $g^+ = 80°$, $g^- = -80°$	300	[92]

case, a "meso" or "racemic" sequence does not change the RIS parameters because of the separation, but they do change the chain structure. We specify an average tacticity by p_{meso} (the proportion of diads that are meso) or p_R (the proportion of side groups that are right-handed). Note that n_{st} random stereochemical sequences are generated, consistent with the average tacticity, with n_{st} sufficiently large to lead to a statistically representative set of stereochemistries; conformational averages are then performed for each stereospecific sequence.

The polymer structures used in the RIS calculations are shown in Fig. 6; for each structure, the bonds that dihedral angles refer to are numbered in red, and the corresponding transfer matrices **U** are tabulated in Table II. We have used data from the literature, collected and referenced in Table II. The matrices **U** depend on parameters $(\eta, \sigma, \sigma', \omega, \ldots)$, which are taken to have the Arrhenius form, e.g., $\eta = \Gamma_\eta e^{-H_\eta/kT}$, $\sigma = \Gamma_\sigma e^{-H_\sigma/kT}$, ..., at *all* temperatures. The Arrhenius activation barriers, e.g., H_η, are typically calibrated by optimization of R_g^2 and $d\ln R_g^2/dT$ for

RIS-modeled chains to match the corresponding values from experimental data [94] at a chosen calibration temperature T_{cal} (Table II). In our MC simulations, we use RIS parameters calibrated using data on melts, for PS and PE, where such data are available; for PMMA, PDMS, and PPG-DME, however, we instead use data calibrated on theta solutions. We expect the M-dependent trends to be the same for theta solutions and for melts, even though the overall chain dimensions vary slightly depending on the nature of the packing between the specific polymer and solvent(s) [95,96].

1. Calculated quantities

The gyration tensor $\mathbf{Q}_\nu$ for a given conformation ν is calculated using the position vectors $\boldsymbol{r}^i$ of the backbone atoms

$$\mathbf{Q}_{\alpha\beta,\nu} = \frac{1}{n_a} \sum_{i=1}^{n_a} (r_\alpha^i - \bar{r}_\alpha)(r_\beta^i - \bar{r}_\beta), \tag{B8}$$

where $\bar{r} = (1/n_a) \sum_i r^i$. Note that individual conformations ν rarely have spherical mass distributions $\mathbf{Q}_\nu$, but they are usually anisotropic and have a biaxial shape similar to a flattened prolate ellipsoid [58]. This gyration tensor $\mathbf{Q}_\nu$ refers to point atoms. To calculate the physical gyration tensor, we incorporate the finite volume of the backbone atoms and associated side groups. For simplicity, we center all side-group volumes on the backbone atoms and calculate the corresponding backbone atom volume V_a as

$$V_a = \frac{4}{3} \pi \sigma_{\mathrm{eff},a}^3, \tag{B9}$$

$$\sigma_{\mathrm{eff},a}^3 = \sum_{j=1}^{m_a} \sigma_{j,a}^3, \tag{B10}$$

where $\sigma_{j,a}$ is the van der Waals radius of the jth of m_a nonhydrogen atoms in backbone atom group a and its associated side groups. The volumes can be found in Ref. [102]. We ignore hydrogen atoms, which have small volumes and relatively small van der Waals energies. The position and respective size of the effective van der Waals volumes are shown as blue spheres in Fig. 6. The corrected gyration tensor $\mathbf{Q}^c$ is given by

$$\mathbf{Q}^c = \mathbf{Q} + \mathbf{I} \frac{1}{3N} \sum_{a=1}^{N} \sigma_{\mathrm{eff},a}^2, \tag{B11}$$

where $\mathbf{I}$ is the identity tensor.

We quantify the shape of molecules by averages of the eigenvalues $\lambda_{i,\nu}^2$ of $\mathbf{Q}_\nu^c$ for given conformations ν,

$$\mathbf{Q}_\nu^c \equiv \begin{pmatrix} \lambda_{1,\nu}^2 & 0 & 0 \\ 0 & \lambda_{2,\nu}^2 & 0 \\ 0 & 0 & \lambda_{3,\nu}^2 \end{pmatrix}, \tag{B12}$$

and order the eigenvalues of $\mathbf{Q}^c$ according to

$$\lambda_{1,\nu}^2 < \lambda_{2,\nu}^2 < \lambda_{3,\nu}^2. \tag{B13}$$

We thus calculate the averages

$$\lambda_i^2 \equiv \langle \lambda_{i,\nu}^2 \rangle = \frac{1}{n_\nu} \sum_a^{n_\nu} \lambda_{i,\nu}^2, \tag{B14}$$

from many ($n_\nu \sim 10^5 – 10^6$) configurations obtained via MC calculations performed using the Metropolis algorithm to approximate a thermal average. For stereocomplex chemistries, we also average over many representative sequences n_{st} to approximate a specified average tacticity. The radius of gyration is calculated as

$$R_g^2 = \langle \mathrm{Tr} \mathbf{Q}^c \rangle = \sum_{i=1}^{3} \lambda_i^2, \tag{B15}$$

and the average end-to-end distance is given by

$$R_e^2 = \langle |r_N - r_1|^2 \rangle. \tag{B16}$$

The characteristic ratio C_n of a chain with n_b bonds is defined as

$$C_n = \frac{R_e^2}{n_b b_{\mathrm{eff}}^2}, \tag{B17}$$

where the effective bond size $b_{\mathrm{eff}} = \sqrt{\sum_{j=1}^{J} b_j^2}$ is the harmonic mean over b_j for each bond j in the repeat unit (i.e., the monomer). There are typically $J = 1, 2,$ or 3 bonds per monomer. There are several conventions for defining b_{eff} for polymers with multiple bonds per monomer; an alternative choice [50] is $b_{\mathrm{eff}} = \sqrt{\sum_j b_j^2 \cos^2 \theta_j}$ (the harmonic mean over $b_j \cos \theta_j$).

We quantify the shape anisotropy using the aspect ratio Λ^2, and here, we also study a second anisotropy measure δ, which captures the non-Gaussianity of finite-length polymers:

$$\Lambda^2 = \frac{\lambda_3^2}{\lambda_1^2} \quad \text{aspect ratio}, \tag{B18a}$$

$$\delta = \frac{R_e^2}{6 R_g^2} \quad \text{non-Gaussianity}. \tag{B18b}$$

For a Gaussian chain, $\Lambda^2 = 11.87$ [58,103], while for a thin rod, $\Lambda^2 = [(3L^2)/(4D^2)]$, where D is the diameter of the rod and L is its length. The non-Gaussianity $\delta = 1$ for a Gaussian chain, where $R_e^2 \sim R_g^2 \sim n_b$. For smaller chains for which the persistence length is not vanishingly small compared to the contour length, the end-to-end length typically scales as n_b rather than $n_b^{1/2}$, and $\delta = 1$ breaks down. For example, $\delta = 2/(1 + 1.5/n_a + 1.7/n_a^2)$ for a string of n_a (even) close-packed spheres in a linear array ($\delta = 0.476$ for two spheres and $\delta = 2$ in the infinitely rigid polymer limit). For a wormlike chain (WLC) with persistence length ℓ_p, one finds [104]

$$\langle R_e^2 \rangle = 2 \ell_p L - 2 \ell_p^2 (1 - e^{-L/\ell_p}), \tag{B19}$$

$$\langle R_g^2 \rangle = \frac{1}{3} \ell_p L - 2 \ell_p^2 \left[1 - \frac{\ell_p}{L} + \left(\frac{\ell_p}{L} \right)^2 (1 - e^{-\ell_p/L}) \right], \tag{B20}$$

so

$$\delta\left(\frac{L}{\ell_p} \right) = \frac{1 - \frac{\ell_p}{L}(1 - e^{-L/\ell_p})}{1 - 6\frac{\ell_p}{L}[1 - \frac{\ell_p}{L} + (\frac{\ell_p}{L})^2(1 - e^{-\ell_p/L})]}. \tag{B21}$$

In the flexible limit, the WLC corresponds to a Gaussian chain with Kuhn step $\ell_K = 2\ell_p$.
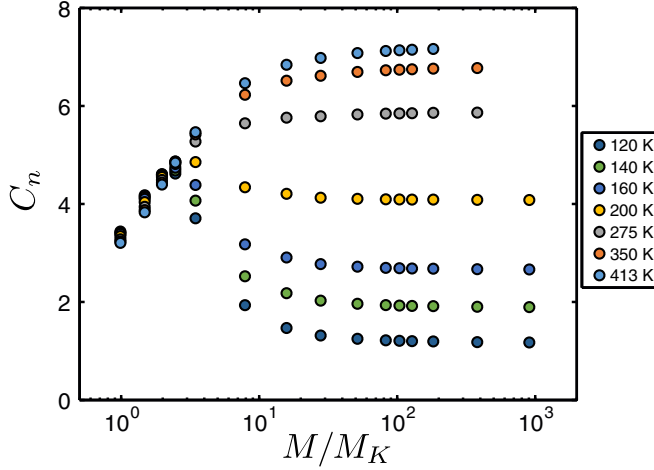
FIG. 7. $C_n(M,T)$ of PDMS calculated using the RIS model for different T, as a function of molecular weight. The maximum at lower T is because the ground state of PDMS in the RIS model is a circle (degenerate helix) [53,60]. Note that the experimental $T_g^\infty = 148$ K, at which point the RIS calculations predict a high prevalence for loops. Experimental chain dimensions have been measured at $T = 298$ K ($C_\infty = 5.8$) and $T = 413$ K ($C_\infty = 6.3$) [105], and the RIS parameters were calibrated at $T = 343$ K [94].

2. Details for specific polymers

The RIS calculations were performed and analyzed in MATLAB, implementing the standard procedure described in Flory's seminal papers [53]. The RIS simulations for PMMA, PS, PPG-DME, and PDMS were performed at temperatures $T_g(M)$, corresponding to the specific molecular weights. Since the full $T_g(M)$ for PE is not known, we perform MC simulations at five different fixed temperatures to investigate the effect of temperature on the structural metrics; we note that the value of $C_\infty = 9.0$ calculated from our simulations for PE at $T = 237$ K is only slightly larger than $C_\infty = 8.3$ determined from experiments at $T = 298$ K [50].

For stereospecific polymers, we use $n_{st} = 10$ for PMMA, $n_{st} = 20$ for PPG-DME, and $n_{st} = 30$ for PS; $p_{meso} = 0.5$ for PS and PMMA; and $p_R = 0.5$ for PPG-DME.

PDMS is different from the other polymers because the Si-O-Si and the O-Si-O angles (Table II) lead to a ground-state conformation of a planar loop with circumference of approximately $n_b = 24$ bonds [53,60]. At the low temperatures near T_g, only few, if any, gauche states are excited, which means that RIS calculations are only reliable for high temperatures, or $n_b < 24$ corresponding to $M \lesssim 88$ g/mol. The calculation of $C_n(M,T)$ at low T thus has a predicted maximum corresponding to the molecular weight at which the ring starts to bend back on itself, as shown in Fig. 7. Recall that excluded volume beyond the closest four monomers (two on each side) is not accounted for in RIS models [53], so a fully degenerate all-trans state is an allowable configuration for RIS calculations, which is unphysical. Since gauche states take the conformation out of the plane, only temperatures low enough to allow very few gauche states lead to unphysical configurations that overlap.

APPENDIX C: CONFORMATIONAL STATISTICS FROM RIS CALCULATIONS

As shown in Fig. 3(f), the aspect ratio Λ^2 shows a maximum as a function of M, which is well correlated with the molecular weight $M^\star$ that marks the change in M dependence of $T_g(M)$. Similarly, the non-Gaussianity δ
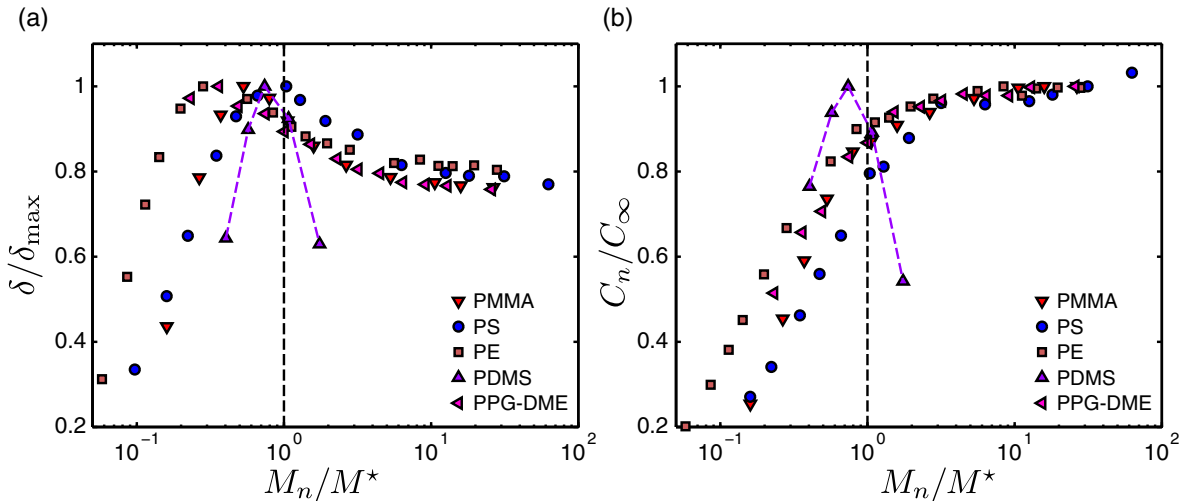

FIG. 8. (a) Calculated non-Gaussianity δ as a function of normalized molecular weight $\delta(M/M^\star)$, normalized by the maximum value δ_{max} from RIS simulations for PMMA, PS, PE, PDMS, and PPG-DME, where $M^\star$ is determined by the scaling in Fig. 2. (b) Calculated characteristic ratio C_n as a function of normalized molecular weight, normalized by C_∞, which we take as the high-M maximum value $C_n^{max} \simeq C_\infty$ (for PS, the maximum value is taken as the average of the three highest M data points). The data for PDMS are qualitatively different from those of the other polymers because of its unusual ground-state-energy loop structure; hence, a dashed line has been added to the PDMS data as a guide to the eye.

TABLE III. T_g^∞ and calibration temperature T_{cal} for the RIS parameters, and molecular weights and number of dihedrals (n_d) corresponding to the maxima of δ and Λ^2 at $M^\star$, from RIS calculations. We use $M^\star$ as determined in Fig. 2(e). Also shown are C_∞^{RIS}, the Kuhn length $\ell_K \equiv C_\infty^{RIS} b_{eff}$ calculated from the simulations at T_g^∞, and the experimental Kuhn length ℓ_K^{exp} reported in the literature [50] (typically for $T \gg T_g$). We have not found a reliable estimate for ℓ_K of PPG-DME. Excluded volume prohibits a reliable calculation of C_∞^{RIS} for PDMS at T_g, as discussed in the text.

	T_g^∞ (K)	T_{cal} (K)	$M(\delta^{max})$ (g/mol)	$n_d(\delta^{max})$	$M(\Lambda_{max}^2)$ (g/mol)	$n_d(\Lambda_{max}^2)$	$M^\star$ (g/mol)	$n_d^\star$	C_∞^{RIS}	ℓ_K (nm)	$\ell_K^{exp}(T)$ (nm)
PDMS	148	343	326	6	474	10	441	11	$\cdots$		1.14 (298 K)
PPG-DME	197	300	162	6	684	33	450	14	5.3	0.8	$\cdots$
PMMA	387	300	1002	7	1502	27	1889	38	12.1	1.9	1.53 (490 K)
PE	200	433	282	17	562	37	1000	107	9.0	1.4	1.54 (298 K)
PS	374	300	1721	32	3177	60	1661	31	12.8	2.0	1.78 (413 K)

also shows a maximum as a function of M, observed at $M \approx M^*$, as shown in Fig. 8. Figure 8(b) shows the normalized values of the Flory characteristic ratio $C_n(M/M^\star)/C_\infty$, where C_∞ represents the high-M value. As shown in Fig. 3, we find that $C_n(M)$ and $T_g(M)$ demonstrate similar behavior for PMMA, PS, PE, and PPG-DME. Mirigian and Schweizer [36] reasoned that a polymer glass can be effectively treated as a hard-sphere glass with a number of interaction sites that depend on the conformation and, more specifically, $C_n(M)$. This led them to conclude that $C_n(M)$ and $T_g(M)$ could show similar behavior. We note, however, that this similarity is not observed for PDMS because of the loop formation at low temperatures near $T_g(M)$ [60].

We have shown [Fig. 3(f)] how the maximum in Λ^2 and the corresponding change in $C_n(M)$—for PMMA, PS, PPG-DME, and PE—are due to chain folding when the molecular weight exceeds M^*. The chain folding is also reflected in the maximum in $\delta(M)$, which occurs near but somewhat below M^*, as shown in Fig. 8(a). However, the data for Λ^2, $\delta(M)$, and $C_n(M)$ for PDMS do not follow the same trends, and the observed maxima are instead due to the formation of loops; these maxima are located close to M^* for all three metrics. Table III provides a summary of our RIS simulation data, together with a comparison with

the corresponding experimental results. The table lists the molecular weights and the number of dihedrals n_d corresponding to δ_{max} and Λ_{max}^2, together with the respective values at $M^\star$; our calculated values of the Flory characteristic ratio C_∞^{RIS} and the Kuhn length l_K together with the experimentally determined l_K; and the experimental calibration temperature.

To illustrate the effects of M and temperature on chain conformations, we study PE by calculating $\Lambda^2(M)$, $C_n(M)$, and $\delta(M)$ for a range of temperatures T. Figure 9(a) shows that $\delta(M)$ at low T follows the results for an all-trans chain configuration with few or no excited gauche states. The semiflexible wormlike chain model for $T = 298$ K shows that the high-M behavior approaches the flexible chain limit $\delta = 1$ for a Gaussian chain. In between the limiting rodlike and flexible regimes, δ has a maximum, indicating how chains fold due to excited (gauche) dihedral states. In the high-M limit, $\delta \to 1$ and $\Lambda^2 \to 11.9$, characteristic of a Gaussian chain [58]. The maxima in $\delta(M)$ shift slightly to larger M for lower temperatures, as expected. Figure 9(b) shows the behavior of $C_n(M)$; the increasing fraction of trans states at the lowest temperatures leads to a significant increase in C_n within regimes II and III. Figure 9(c) shows that the aspect ratio Λ^2 behaves similarly for the three highest T, including an increase at low M within regime I; a
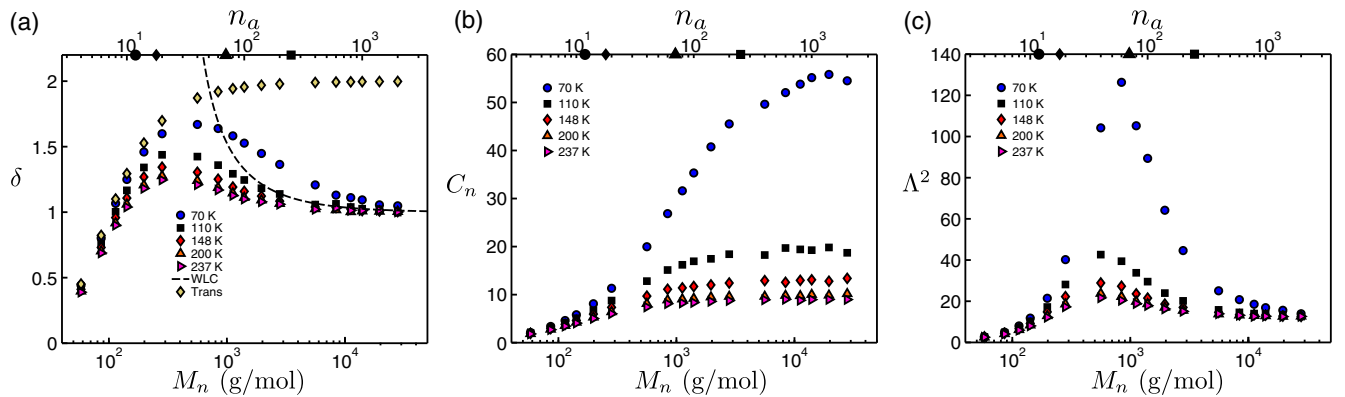

FIG. 9. Chain conformation metrics δ, C_n, Λ^2 for PE at different temperatures. Panel (a) also includes calculations for the all-trans state of PE and a wormlike chain model with persistence length $\ell_p = \ell_K/2$, with Kuhn step $\ell_K = 1.54$ nm, corresponding to $T = 298$ K. The experimentally measured values are $C_\infty(298 \text{ K}) = 8.26$, $C_\infty(413 \text{ K}) = 7.38$ [50].
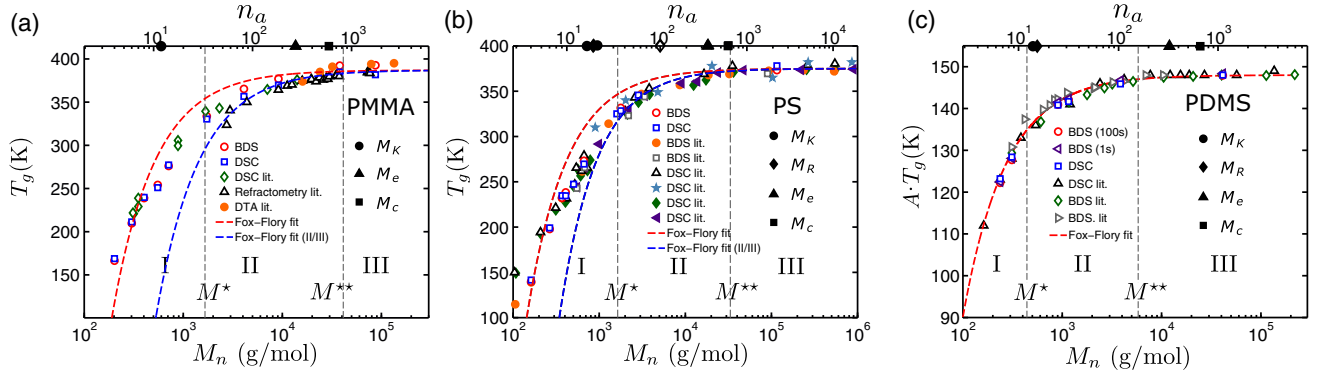
FIG. 10. T_g as a function of number-averaged molecular weight M_n and the number of backbone atoms n_a. Data from BDS, DSC, and rheology are combined with literature data for PMMA [44,107,108], PS [12–14,109,110], and PDMS [13,47,111]. The absolute value of $T_g(M)$ can vary slightly between different studies because of the variation in experimental techniques, T_g definition, or polymer specification. For PDMS, these differences are more pronounced since T_g is a weaker function of M_w ($\Delta T_g \simeq 40$ K) than for PMMA or PS ($\Delta T_g \simeq 200$ K). Thus, a scaling factor $A \sim 1$–1.03 is used to collapse different data sets onto $AT_g(M)$. The PDMS data incorporate T_g determined from two different definitions, $\tau_\alpha = 100$ s and 1s, which slightly change T_g without significantly changing $T_g(M)$. The symbols on the upper abscissa denote the Kuhn molecular weight (filled black circle; PMMA [112], PS [20]), the "dynamical" or Rouse molecular weight M_R (filled black diamond; PS and PDMS [20], diamond PS; using an alternative M_R definition [52]), the entanglement molecular weight M_e (filled black up-pointing triangle; PMMA [50], PS and PDMS [90]), and the critical molecular weight M_c (filled black square; PMMA [113], PS and PDMS [90]). Dashed lines are fits to the Fox-Flory expression $T_g = T_g^\infty - a/M$, using different ranges for the fits. Here, n_a denotes the number of backbone atoms, and $M^\star$ and $M^{\star\star}$ separate regimes I–III.
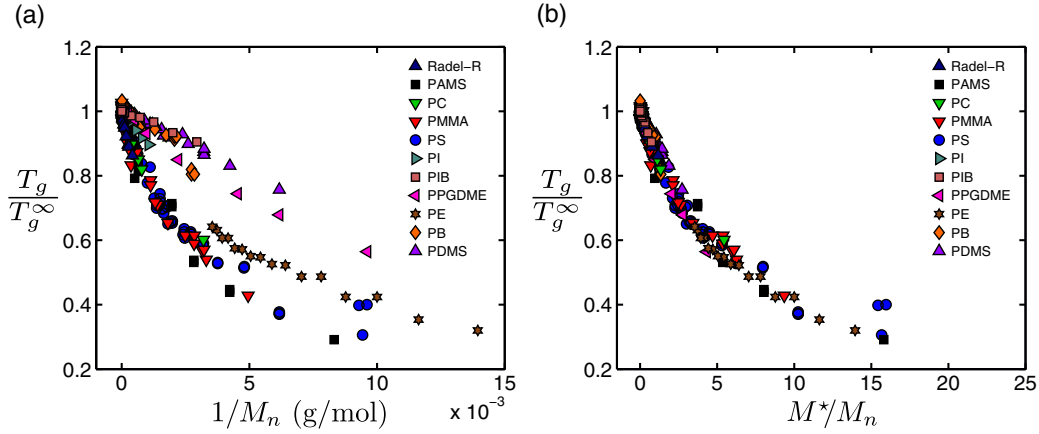

FIG. 11. Fox-Flory plot for 11 polymers showing (a) T_g/T_g^∞ vs $1/M$ and (b) T_g/T_g^∞ vs $M^\star/M$. Fox-Flory behavior implies a straight line, $T_g - T_g^\infty \sim 1/M$.

maximum near the regime I–II crossover where the chain starts to fold; and a decrease towards the Gaussian limit where $\Lambda^2 = 11.87$ [106] for high M. The maximum is more prominent for the lowest T, and it occurs at larger values of M because of the corresponding higher chain stiffness.

APPENDIX D: FOX-FLORY DESCRIPTION OF $T_g(M)$ FOR POLYMERIC GLASS FORMERS

Figure 10 shows $T_g(M)$ data for PMMA, PS, and PDMS [also shown in Figs. 1(a)–1(c)] together with fits to the standard Fox-Flory expression, $T_g = T_g^\infty - a/M$. For each polymer, the data were either fit over the full data range (regimes I–III; dashed red line) or over a limited data range

(regimes II and III; dashed blue line). We find that a Fox-Flory expression cannot describe either PMMA or PS across all three regimes; a Fox-Flory expression can reasonably approximate regimes II and III, even though a semilogarithmic fit [$T_g = A_{II} + b_{II}\log_{10}(M)$] provides a better fit within regime II. The more flexible PDMS can also be described within regimes I and II by semilogarithmic fits as shown in Fig. 1(c), but contrary to the behavior of the less-flexible polymers PS and PMMA, a Fox-Flory expression can alternatively describe PDMS adequately across all three regimes I–III, as shown in panel (c). Since data in the literature are often plotted as T_g vs $1/M$, we also illustrate the behavior for the 11 polymers in this representation in Fig. 11(a), where T_g has been normalized by its

long chain-length value T_g^∞ to facilitate comparisons. The same data are also showed in Fig. 11(b), with the abscissa rescaled by $M^\star$ to aid the comparison to Fig. 2(e).

APPENDIX E: POLYMER DATA AND LITERATURE REFERENCES

The $T_g(M_n)$ literature data included in Figs. 2(a)–2(c) are as follows: PMMA (• [107], up-pointing triangle [108], diamond [44]), PS (filled black circle [13], up-pointing triangle [14], filled black circle [12], filled black diamond [114], left-pointing triangle [110]) and PDMS (diamond [13], up-pointing triangle [47], right-pointing triangle [111]). The $T_g(M)$ literature data included in Figs. 2(d) and 2(e) are as follows: Radel-R [115], PC [116,117], PI [118], PIB [119], PE [49], PB [13,120], and PPG-DME [121] [for PPG-DME, the T_g value for PPG of $M_n = 4000$ g/mol ($n = 69$) is included as a good approximation of the long-chain behavior for PPG-DME since the influence of the hydroxyl end groups is marginal for this high molecular weight [121–123]]. All data are number-averaged molecular weight M_n except for Radel-R and one data set for PS [114] for which only M_w is available.

Table IV includes data for the 11 polymers included in the master curve in Fig. 2. The table includes the monomer repeat molecular weight M_o, the conformer molecular weight M_ϕ and volume V_ϕ (both defined below), the molecular weight of the chain ends M_{end}, the Kuhn molecular weight M_K, the Rouse (or dynamic bead) molecular weight M_R, the entanglement molecular weight M_e, the critical molecular weight M_c (at which entanglements are effective), the long-chain limit of the glass-transition temperature, T_g^∞, the long-chain limit of the Flory characteristic ratio, C_∞, the molecular weight $M^\star$ that separates regimes I and II in the $T_g(M)$ behavior, and the molecular weight $M^{\star\star}$ that separates regimes II and III. For the majority of polymers, where significant data were available in all three regimes, $M^\star$ was determined by fitting data within regimes I and II to the form $T_g = A_{\text{I,II}} + B_{\text{I,II}} \log_{10} M$, while $M^{\star\star}$ was determined as the molecular weight above which $T_g \simeq T_g^\infty$. For polymers where data were mainly, or only, available within two of the regimes (PI, PIB, PPG-DME, and Radel-R), $M^\star$ was instead determined by optimization to the master curve formed by the other polymers. For PE, data were only available within regime I, and $M^\star$ was thus determined by optimization to regime I data of the other polymers. The temperature at which C_∞ was determined is noted in the table. For PAMS, PIB, PS, and PC, the literature values for M_R were determined from mechanical spectroscopy [124], while for PB, PDMS, PI, and PPG-DME, the M_R values were determined from fast field-cycling nuclear magnetic resonance (FFCNMR) [125]. In both cases, the data were modeled as a superposition of α-relaxation and Rouse relaxation spectrum contributions, where a linear

superposition of either moduli or compliances (susceptibilities) was performed.

To calculate M_ϕ and V_ϕ, we count the relevant number of conformational DOF, or conformers, per monomer, where we include the number of conformers n_ϕ that sweep out significant volume during a rearrangement. A dihedral rotation is counted as a conformer whether it is situated in the backbone or in a side chain, and we also count an aromatic ring rotation, a cyclohexane group rotation, or a chair/boat conformational change as a conformer. However, we ignore groups whose motions displace small volumes, such as methyl groups, aromatic ring rotations within the backbone (such as in PET), and dihedrals involving small groups such as $CH = CH_2$ in 1,2 PB, or $O\text{-}CH_3$ in PMMA. The mass per conformer M_ϕ is subsequently defined as the mass per monomer (or polymerization unit) M_o divided by the total number of conformers per monomer n_ϕ, as $M_\phi = M_o/n_\phi$. Thus, M_ϕ averages the conformational DOF within the monomer, representing a particular polymer chemistry. The average volume per conformer $V_\phi = V_{\text{mon}}/n_\phi$ is calculated from the sum V_{mon} of the van der Waals volumes of all groups in the monomer, tabulated in Ref. [131].

Table V provides data for M_ϕ, the number of conformers per monomer n_ϕ, M_o, V_ϕ, and T_g^∞ for a wider range of polymers with C-, C-C-O-, Si-, or Si-O-based backbones, as shown in the $T_g(M_\phi)$ plot in Fig. 2(f).

As a complement to Fig. 2(e), Fig. 12(a) shows the dependence of T_g^∞ on V_ϕ (in Å^3) for the polymers in Table V, demonstrating a rough correlation $T_g^\infty = T_V + B_V \log_{10}(V_\phi)$, where T_V depends on the sequence and species of atoms in the polymer backbone, and $B_V \sim 300$ K for carbon-based backbones but, at least for the Si-based backbones, appears to be somewhat smaller. Note that $M^\star$ is plotted versus M_ϕ in Fig. 12(b) to investigate the inter-relationship between the two characteristic molecular weights. We find $M^\star \approx 24 M_\phi$, consistent with the crossover between regimes I and II occurring when the chain has reached a length corresponding to about 24 conformers.

Figure 13(a) shows $T_g^\infty(M)$ for the 11 polymers of Table IV, either in a (a) semilogarithmic or (b) linear plot. The comparison between the two panels demonstrates that the relationship between T_g^∞ and M can, to a good approximation, be described using either a semilogarithmic or linear form [see inset in Fig. 2(e)]. We have less confidence in M^* for those polymers for which data covering all three regimes are not available (PE, PI, PIB, PC, and Radel-R); these data are shown as open symbols in Figs. 12(b) and 13.

Figure 14(a) shows the relation of the packing length p or Kuhn length ℓ_K vs T_g^∞. The packing length is defined as the high-molecular-weight limit of $p = V/R_g^2$, where V is the polymer volume. If we (naively) approximate a Kuhn volume as a cylinder of length ℓ_K and diameter d,

TABLE IV. Characteristic data for the polymers used in Fig. 2. All parameters included in the table are described in the text. Masses are in g/mol and are defined in Table I. In each case, the end-group mass M_{end} chosen is for a typical polymerization chemistry.

Number[a]	Polymer	M_o	M_ϕ	$V_{\phi l}/\text{Å}^3$	M_{end}	M_K	M_R		$M_e/10^3$		$M_c/10^3$		$T_g^{\infty,b}/\text{K}$	$C_\infty^c (T/\text{K})$		$M^\star/10^3$	$M^{\star\star}/10^3$
1	PE	28	14	17	2	168	252	[126]	0.98	[50]	3.5	[50]	200	8.3 (298) 7.4 (413)	[50]	1.0	⋯
2	1,4-PB	54	18	21	30	113	500	[125]	2.9	[50]	4.5	[127]	175	4.6 (298)	[50]	0.47	2.3
20	PPG-DME	58	19	20	46	⋯	150	[125]	2.8	[105]	7	[128]	197	5.1 (298)	[129]	0.45	6.0
5	PIB	56	28	34	⋯	274	200	[124]	6.9	[50]	13	[50]	210	6.7 (298) 6.6 (413)	[50]	0.25	30.9
9	1,4-PI	68	34	26	⋯	129	1000	[125]	3.9	[50]	10	[127]	213	5.2 (298)	[50]	0.6	100.0
11	PMMA	100	50	47	2	598	⋯		13.6	[50]	30	[50]	387	8.2 (413)	[50]	1.9	41.2
12	PS	104	52	54	58	720	850[d] 5000	[52,124]	16.6	[50]	35	[127]	374	9.6 (413)	[105]	1.7	33.3
14	PAMS	118	59	62	2	960	730	[124]	13.3	[50]	28	[50]	438	10.1 (473)	[127]	1.9	17.9
15	PC	254	85	60	⋯	127	490	[124]	1.3	[105]	⋯		426	2.4 (473)	[130]	1.7	20.0
17	RADEL-R	400	134	347	⋯	113	⋯		1.6	[50]	⋯		502	2.0 (298)	[115]	2.8	⋯
26	PDMS	74	37	38	162	381	600	[125]	12	[50]	25	[50]	148	5.8 (298) 6.3 (413)	[105]	0.44	5.8

[a]Numbers in the first column correspond to the entries in Table V.
[b]References for T_g^∞ are given in Table V.
[c]C_∞ is given at the indicated temperatures.
[d]Two values for the dynamic bead (Rouse) mass M_R are given for PS, as reported in the literature: 850 g/mol [124] or 5000 g/mol [52].

TABLE V. Table of molecular weights (in g/mol) and volumes per conformer, ordered in increasing mass per total conformer (i.e., including the side groups but excluding methyl groups) and separated according to backbone chemistry.

No.	Polymer	Acronym	M_ϕ	n_ϕ	M_0	V_ϕ (Å³)	T_g^∞ (K)	Ref.	p (Å)	ℓ_K (Å)	T_{char}^a (K)	Backbone
1	Poly(ethylene)	PE	14	2	28	17	200	[49]	1.39	1.54	298	C
2	1,4-poly(butadiene)	1,4-PB	18	3	54	63	175	[*]	2.44	8.28	298	C
3	Poly(propylene)[b]	PP	21	2	42	51	266	[132]	1.12	2.88	298	C
4	Poly(vinylethylene)[b]	PVE	27	2	54	63	273	[133]		14		C
5	Poly(isobutylene)	PIB	28	2	56	68	210	[*]	3.18	12.50	298	C
6	Poly(vinyl chloride)[b]	PVC	31	2	63	49	354	[134]				C
7	Poly(ethylene terephthalate)	PET	32	6	192	161	346	[135]	1.99	14.91	548	C
8	Poly(vinylidene fluoride)	PVDF	32	2	64	43	238	[136]				C
9	1,4 poly(isoprene)	1,4-PI	34	2	68	79	213	[*]	2.69	9.34	298	C
10	Poly(vinylidene chloride)	PVDC	49	2	97	63	255	[136]				C
11	Poly(methyl methacrylate)[b]	PMMA	50	2	100	95	387	[*]	3.77	15.30	413	C
12	Poly(styrene)[b]	PS	52	2	104	107	374	[*]	3.92	17.80	413	C
13	Poly(phenylene sulfide)	PPS	54	2	108	94	348	[137]				C
14	Poly(α-methyl styrene)[b]	PAMS	59	2	118	124	438	[*]	3.61	20.43	473	C
15	Poly(carbonate) of bisphenol A	PC	85	3	254	239	426	[*]	1.69	18.43	473	C
16	Poly(ether ether ketone)	PEEK	92	3	276	257	437	[138]				C
17	Poly(4, 4′-biphenol-alt-dichlorodiphenyl sulfone)	Radel-R	111	4	444	347	502	[*]	1.66			C
18	Poly(phenyl ether)	PPE	120	1	120	81	484	[55]				C
19	Poly (ethylene glycol)	PEG	15	3	44	42	213	[139]	1.95	9.71	353	C-C-O
20	Poly (propylene glycol) dimethyl ether[b]	PPG-DME	19	3	58	59	197	[*]	2.77			C-C-O
21	Poly(di-n-hexylsilane)	PDHS	18	11	198	243	221	[140]				Si
22	Poly(propylmethylsilane)[b]	PPrMS	29	3	86	107	245	[141]				Si
23	Poly(trifluoropropylmethylsilane)[b]	PTFPrMS	47	3	140	120	270	[141]				Si
24	Poly(cyclohexylmethylsilane)[b]	PCHMS	63	2	125	188	366	[142]				Si
25	Poly(phenylmethylsilane)[b]	PPMS	120	1	120	126	390	[142]				Si
26	Poly(dimethylsiloxane)	PDMS	37	2	74	76	148	[*]	4.06	11.40	298	Si-O
27	Poly(methylphenylsiloxane)[b]	PMPS	68	2	136	135	228	[143]				Si-O

[a]Polymer packing length p and Kuhn step ℓ_K are characterized at temperature T_{char}.

[b]Stereoisomeric polymers are quoted for atactic materials. In some cases, the tacticity is known and published, while in other cases, it is not known. Here, T_g for PE was determined by extrapolation from Ref. [49], while for polymers with references noted as [*], T_g^∞ was determined as the high-M limit of data referenced and shown in Fig. 2.
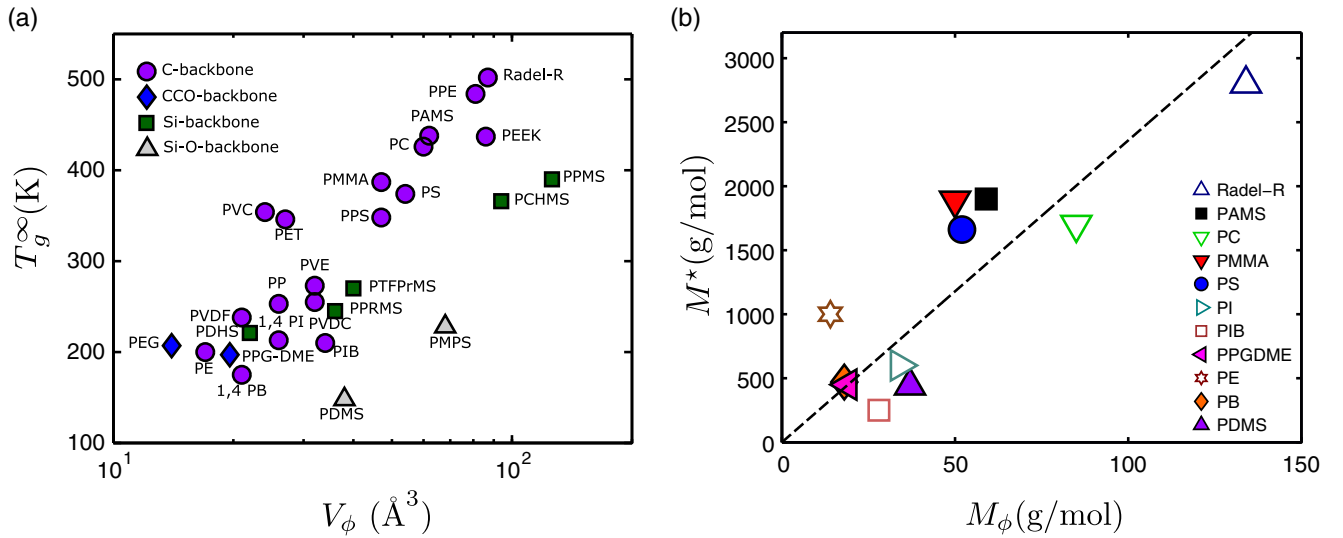

FIG. 12. (a) T_g^∞ vs V_ϕ for the polymer systems in Table V. The different symbols or colors refer to different backbone chemistries. (b) $M^\star$ vs M_ϕ. The dashed line is a linear fit yielding $M^\star \simeq 24 M_\phi$. Open symbols in panel (b) denote polymers with less certainty in $M^\star$ due to data that do not cover all three regimes in $T_g(M)$.
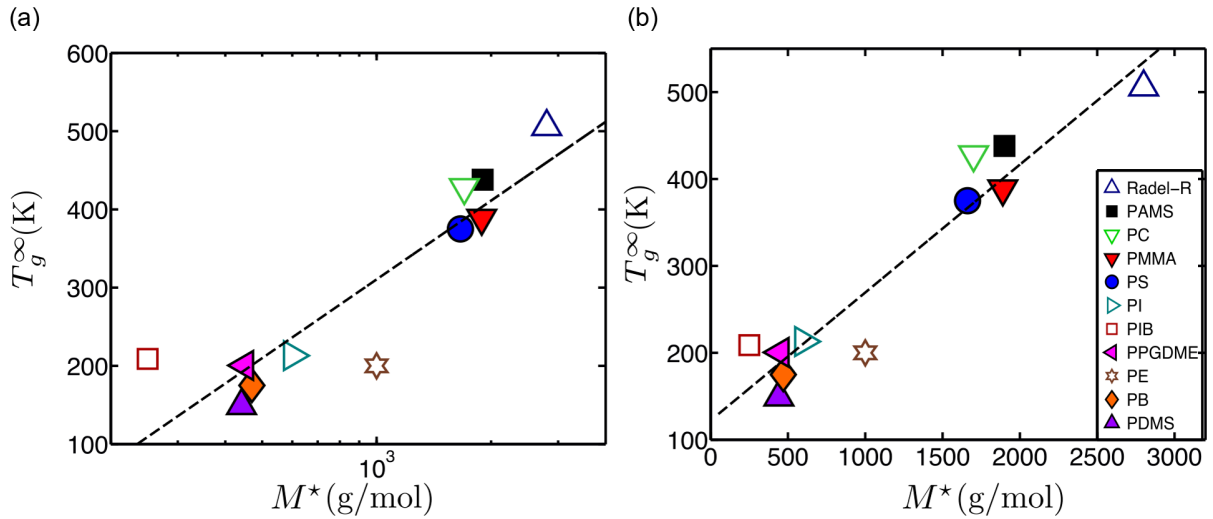
FIG. 13. T_g^∞ vs M^* in a (a) semilogarithmic and (b) linear plot. Open symbols denote polymers with less certainty in M^* due to data that do not cover all three regimes in $T_g(M)$.
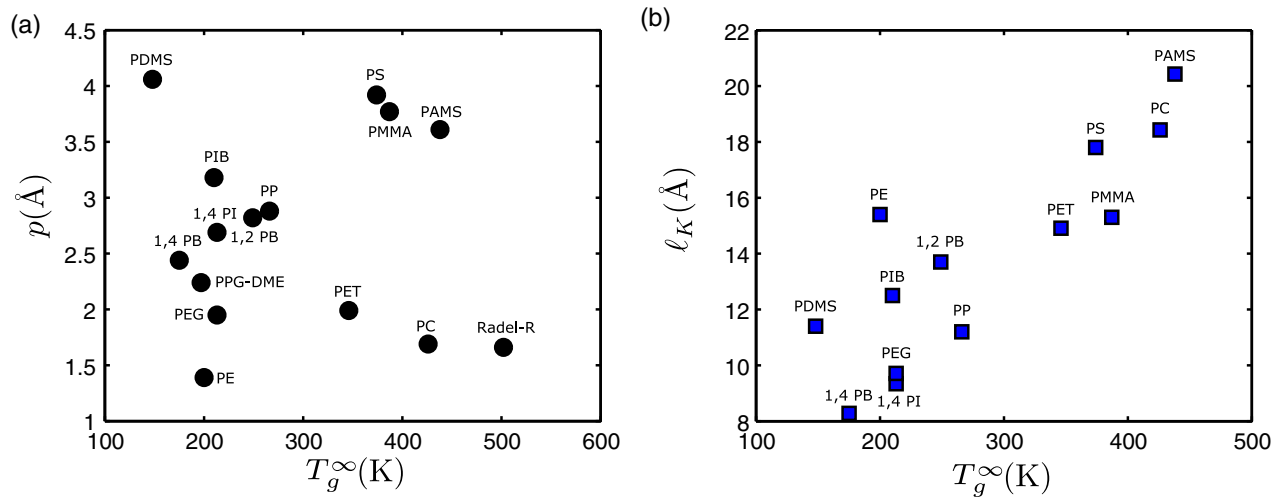

FIG. 14. Relation between T_g^∞ and the packing length p and the Kuhn step ℓ_K for PE 1,4-PB, PP, 1,2-PB, PIB, PET, 1,4-PI, PMMA, PS, PAMS, PC, Radel-R (only p), PEG, PPG-DME (only p), and PDMS.

we find $p \sim d^2/\ell_K$. The packing length quantifies the balance between intrachain and interchain interactions, and has a strong correlation with metrics such as the entanglement or critical molecular weights M_e and M_c [105]. Figure 14(a) shows no obvious correlation between p and T_g^∞. However, stiffer chains characterized by larger Kuhn lengths typically have higher T_g^∞, as shown in Fig. 14(b).

APPENDIX F: DATA FOR NONPOLYMERIC "RIGID" GLASS FORMERS

To investigate the molecular-weight-dependent T_g behavior for nonpolymeric rigid glass formers with as few conformational degrees of freedom as possible, we follow Ref. [66] and choose a series of mainly aromatic, carbon-based molecules, which do not contain alkane chains of more than three carbons. We expect all the chosen systems to interact in a similar manner, which allows for direct comparisons. The T_g values were taken from Ref. [66] (with the addition of bisphenol A diacetate, number 10 in Table VI). Table VI contains the molecular structure, chemical name, molecular weight M, and T_g. Figure 15 shows $T_g(M)$ for the rigid molecules in a semilogarithmic (a), linear (b), or double-logarithmic (c) representation; the semilogarithmic plot [Fig. 15(a)] provides the best fit. We stress that even though a semilogarithmic fit describes our chosen data best, this is not necessarily the case for other series of rigid molecules.

TABLE VI. Table of data compiled by Larsen and Zukowski [66], with the addition of molecule 10, for rigid, mainly aromatic, small molecular glass formers. These are ordered according to increasing molecular weight.

	Structure	Name	M (g/mol)	T_g (K)
1		Cyclohexene	84.2	81
2		Toluene	92.1	113
3		Ethylbenzene	106	111
4		Iso-propylbenzene	120	127
5		4-tert-butyl-pyridine (4-TBP)	135	166
6		Cresyl-glycidyl-ether (CGE)	164	204
7		Dimethylphthalate (DMP)	194	195
8		Ortho-terphenyl	230	244
9		Triepoxide N-N-diglycidyl-4-glycidyloxyaniline (DGGOA)	277	244
10		Bisphenol A diacetate	312	257
11		Phenolphthalein-dimethylether (PDE)	340	294
12		Kresolphtalein-dimethylether (KDE)	376	311
13		Diglycyl ether of bisphenol A (DGEBA)	380	257
14		1,3,5-tri-1-naphthyl benzene	456	342

Novikov and Rössler studied $T_g(M)$ [144] for a wide range of nonpolymeric (and some oligomeric) glass formers of different chemistries and interactions. Their entire data set could be fit to a power law $T_g(M) \sim M^\alpha$, with $\alpha \approx 0.5$. However, a subset of aromatic molecules was best fit by $\alpha \approx 0.7$. For comparison, our data [Fig. 15(c)] yield $\alpha \approx 0.7$.
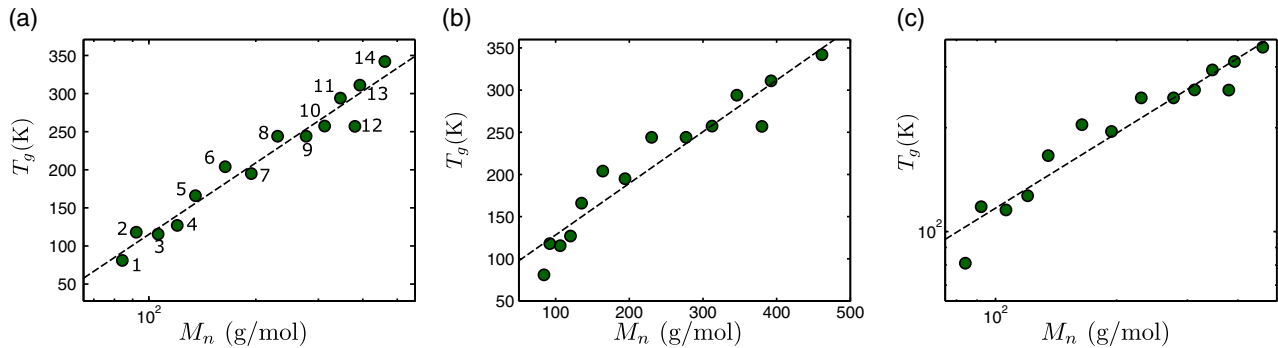
FIG. 15. T_g as a function of molecular weight M for rigid molecules from Table VI, as shown in semilogarithmic (a), linear (b), and double-logarithmic (c) representations. The dashed lines are linear fits to the data in each representation, and they provide a guide to the eye for the evaluation of the degree of linearization provided in each case.

APPENDIX G: SECONDARY β AND γ RELAXATIONS

1. General

Secondary relaxations are generally observed in polymer glasses. For the 11 polymer systems investigated in detail in this work, secondary relaxations have been experimentally reported in all except Radel-R for which only very few detailed spectroscopic investigations have been performed [115,145]; other polysulfones show secondary relaxations [146], suggesting that they would also be found in Radel-R by detailed experimental investigation. The other 10 polymers all demonstrate secondary relaxations; see, e.g., PAMS [147], PC [148–150], PMMA [42,151,152], PS [153], PI [154,155], PIB [156], PPG-DME [157], PE [158,159], PB [74,75,160], and PDMS [76,111].

Depending on the particular polymer chemistry and the experimental technique used [e.g., BDS, nuclear magnetic resonance (NMR), neutron spin echo (NSE), and dynamic light scattering], the experimental sensitivity to specific molecular motions can vary significantly. However, secondary relaxations in glassy polymers are typically assigned to molecular rearrangements that include both backbone and side-group rotations [42,151], even though the exact rearrangements are often difficult to determine and literature assignments often vary depending on the experimental or computational technique used or the dynamic range investigated. Much work has focused on long-chain PMMA and PB. Detailed NMR and BDS studies on PMMA [42,151,152] concluded that the molecular motions involved in the β relaxation are complex and involve coupled small- and large-angle motions of both the side and main chains. For PB, a combined NSE and BDS study found evidence for cooperative rotations involving several units along the chain and concluded that the β relaxation originated in intramolecular rotational motion of cis and trans chain units [42].

The role of conformational dihedral transitions in the relaxation dynamics of polymers was studied by computer simulations [43,69,161]. Atomistic MD simulations of

PB [43,161] demonstrated the strong link between conformational dihedral rotation and the β relaxation, and simulations of PPG-DME [16] demonstrated the importance of intramolecular dihedral reorientations in controlling relaxation dynamics.

We present a detailed study of the molecular-weight-dependent secondary relaxation behavior of PMMA and PB, since for these two polymer systems, we can access the secondary β and γ relaxations across the full molecular weight range.

2. Activation enthalpies for β and γ relaxations

The M-dependent activation enthalpies for β (circles) and γ (squares) relaxations within the glassy state are shown in Fig. 16 for PMMA and PB. As described in Sec. VI, the β- and γ-relaxation enthalpy data for PB are obtained from BDS measurements, complemented with literature data [70–75], shown in Fig. 5 as $\Delta H / \langle \Delta H_\gamma \rangle$. In this representation, PMMA and PB behave similarly, despite the different chain flexibilities of PMMA and PB. The more flexible nature of PB is reflected in a smaller
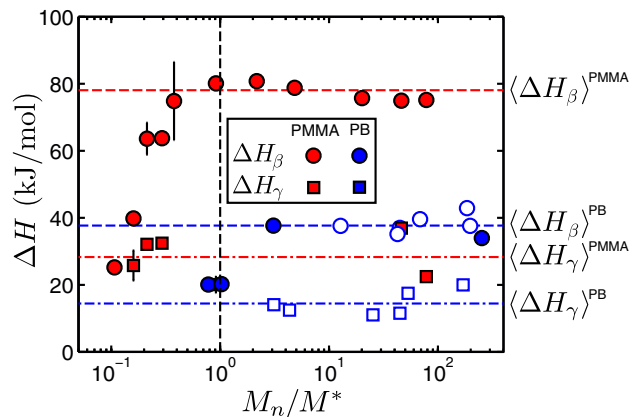

FIG. 16.   Activation enthalpies $\Delta H_{\beta,\gamma}(M)$ for PMMA and PB. Circles denote ΔH_β and squares denote ΔH_γ. PB data from literature [70–75] are shown in open symbols.

TABLE VII. Weight-averaged molecular weight M_w, polydispersity index (PDI=M_w/M_n, where M_n is the number-averaged molecular weight), fit parameters from VFT fits of τ_α data to $\tau_\alpha = \tau_0^\alpha \exp DT_0/(T - T_0)$, and fit parameters from Arrhenius fits of τ_β and τ_γ data to $\tau_\beta = \tau_0^\beta \exp \Delta H_\beta/RT$, for the PMMA data in Fig. 1.

M_w (g/mol)	PDI	$\log_{10}(\tau_0^\alpha/\text{s})$	D	T_0 (K)	$\log_{10}(\tau_0^\beta/\text{s})$	ΔH_β (kJ/mol)	$\log_{10}(\tau_0^\gamma/\text{s})$	ΔH_γ (kJ/mol)
202	1	−16.1	13.5	126.0	−14.2	25.2	⋯	⋯
302	1	−14.3	10.0	165.7	−13.1	39.8	−12.0	26.0
402	1	−13.5	8.7	192.0	−16.0	64.0	−13.4	32.1
660	1.21	−12.5	8.0	205.0	−14.5	63.8	−12.9	32.4
840	1.44	−12.7	9.3	217.0	−16.0	75.0	⋯	⋯
1900	1.10	−12.9	6.9	278.0	−16.0	80.1	−10.6	20.0
4300	1.05	−14.0	6.6	310.0	−15.9	80.8	⋯	⋯
9590	1.05	−12.4	4.7	330.0	−15.5	78.8	⋯	⋯
39500	1.04	−10.9	2.1	366.0	−15.0	75.7	⋯	⋯
90600	1.04	−11.0	2.2	366.0	−14.9	75.0	−12.6	36.9

activation enthalpy (Fig. 16). Note that in Ref. [75], the observed secondary γ relaxations are termed γ_A (in the range $T = 80$–100 K) and γ_B (in the range $T = 50$–65 K).

Table VII summarizes the molecular weights and polydispersities for the PMMA samples studied, as well as the fitting parameters for the VFT and Arrhenius fits of the α, β, and γ relaxations shown in Fig. 1(a).

---

[1] C. A. Angell, K. L. Ngai, G. B. McKenna, P. F. McMillan, and S. W. Martin, *Relaxation in Glassforming Liquids and Amorphous Solids*, J. Appl. Phys. **88,** 3113 (2000).

[2] J. C. Dyre, *Colloquium: The Glass Transition and Elastic Models of Glass-Forming Liquids*, Rev. Mod. Phys. **78,** 953 (2006).

[3] A. K. Doolittle, *Studies in Newtonian Flow. II. The Dependence of the Viscosity of Liquids on Free-Space*, J. Appl. Phys. **22,** 1471 (1951).

[4] R. P. White and J. E. Lipson, *Polymer Free Volume and Its Connection to the Glass Transition*, Macromolecules **49,** 3987 (2016).

[5] J. C. Dyre, T. Christensen, and N. B. Olsen, *Elastic Models for the Non-Arrhenius Viscosity of Glass-Forming Liquids*, J. Non-Cryst. Solids **352,** 4635 (2006).

[6] G. Adam and J. H. Gibbs, *On the Temperature Dependence of Cooperative Relaxation Properties in Glass-Forming Liquids*, J. Chem. Phys. **43,** 139 (1965).

[7] T. G. Fox, Jr. and P. J. Flory, *Second-Order Transition Temperatures and Related Properties of Polystyrene. I. Influence of Molecular Weight*, J. Appl. Phys. **21,** 581 (1950).

[8] J. H. Gibbs and E. A. DiMarzio, *Nature of the Glass Transition and the Glassy State*, J. Chem. Phys. **28,** 373 (1958).

[9] K. Ueberreiter and G. Kanig, *Self-Plasticization of Polymers*, J. Coll. Sci. **7,** 569 (1952).

[10] J. Dudowicz, K. Freed, and J. Douglas, *The Glass Transition Temperature of Polymer Melts*, J. Phys. Chem. B **109,** 21285 (2005).

[11] A. Zaccone and E. Terentjev, *Disorder-Assisted Melting and the Glass Transition in Amorphous Solids*, Phys. Rev. Lett. **110,** 178002 (2013).

[12] J. M. G. Cowie, *Some General Features of Tg-M Relations for Oligomers and Amorphous Polymers*, Eur. Polym. J. **11,** 297 (1975).

[13] J. Hintermeyer, A. Herrmann, R. Kahlau, C. Goiceanu, and E. A. Rössler, *Molecular Weight Dependence of Glassy Dynamics in Linear Polymers Revisited*, Macromolecules **41,** 9335 (2008).

[14] P. Claudy, J. Letoffe, Y. Camberlain, and J. Pascault, *Glass Transition of Polystyrene versus Molecular Weight*, Polym. Bull. **9,** 208 (1983).

[15] J. Colmenero, *Are Polymers Standard Glass-Forming Systems? The Role of Intramolecular Barriers on the Glass-Transition Phenomena of Glass-Forming Polymers*, J. Phys. Condens. Matter **27,** 103101 (2015).

[16] M. Vogel, *Conformational and Structural Relaxations of Poly(ethylene oxide) and Poly(propylene oxide) Melts: Molecular Dynamics Study of Spatial Heterogeneity, Cooperativity, and Correlated Forward-Backward Motion*, Macromolecules **41,** 2949 (2008).

[17] W. Kauzmann and H. Eyring, *The Viscous Flow of Large Molecules*, J. Am. Chem. Soc. **62,** 3113 (1940).

[18] M. Siline and A. I. Leonov, *On the Length of Statistical Segment in Flows of Polymers*, Polymer **43,** 5521 (2002).

[19] C. Jeong and J. F. Douglas, *Mass Dependence of the Activation Enthalpy and Entropy of Unentangled Linear Alkane Chains*, J. Chem. Phys. **143,** 144905 (2015).

[20] Y. Ding, A. Kisliuk, and A. Sokolov, *When Does a Molecule Become a Polymer?*, Macromolecules **37,** 161 (2004).

[21] R. F. Boyer, *The Relation of Transition Temperatures to Chemical Structure in High Polymers*, Rubber Chem. Technol. **36,** 1303 (1963).

[22] V. A. Bershtein, V. M. Egorov, A. F. Podolsky, and V. A. Stepanov, *Interrelationship and Common Nature of the β Relaxation and the Glass Transition in Polymers*, J. Polym. Sci., Polym. Lett. Ed. **23,** 371 (1985).

[23] R. F. Boyer, *Mechanical Motions in Amorphous and Semi-crystalline Polymers*, Polymer **17,** 996 (1976).

[24] R. H. Boyd, *Relaxation Processes in Crystalline Polymers: Molecular Interpretation—A Review*, Polymer **26,** 1123 (1985).

[25] R. H. Boyd, *Relaxation Processes in Crystalline Polymers: Experimental Behaviour—A Review*, Polymer **26,** 323 (1985).

[26] K. Ngai and D. Plazek, *Relation of Internal Rotational Isomerism Barriers to the Flow Activation Energy of Entangled Polymer Melts in the High-Temperature Arrhenius Region*, J. Polym. Sci., Polym. Phys. Ed. **23,** 2159 (1985).

[27] C. Roland, S. Hensel-Bielowka, M. Paluch, and R. Casalini, *Supercooled Dynamics of Glass-Forming Liquids and Polymers under Hydrostatic Pressure*, Rep. Prog. Phys. **68,** 1405 (2005).

[28] G. Floudas, K. Mpoukouvlas, and P. Papadopoulos, *The Role of Temperature and Density on the Glass-Transition Dynamics of Glass Formers*, J. Chem. Phys. **124,** 074905 (2006).

[29] K. Mpoukouvalas, G. Floudas, and G. Williams, *Origin of the α, β, (βα) and "Slow" Dielectric Processes in Poly(ethyl methacrylate)*, Macromolecules **42,** 4690 (2009).

[30] R. Casalini, C. Roland, and S. Capaccioli, *Effect of Chain Length on Fragility and Thermodynamic Scaling of the Local Segmental Dynamics in Poly(methylmethacrylate)*, J. Chem. Phys. **126,** 184903 (2007).

[31] W. Götze and L. Sjögren, *Relaxation Processes in Supercooled Liquids*, Rep. Prog. Phys. **55,** 241 (1992).

[32] K. Schweizer, *Dynamical Fluctuation Effects in Glassy Colloidal Suspensions*, Curr. Opin. Colloid Interface Sci. **12,** 297 (2007).

[33] S. Frey, F. Weysser, H. Meyer, J. Farago, M. Fuchs, and J. Baschnagel, *Simulated Glass-Forming Polymer Melts: Dynamic Scattering Functions, Chain Length Effects, Mode-Coupling Theory Analysis*, Eur. Phys. J. E **38,** 11 (2015).

[34] S.-H. Chong and M. Fuchs, *Mode-Coupling Theory for Structural and Conformational Dynamics of Polymer Melts*, Phys. Rev. Lett. **88,** 185702 (2002).

[35] E. J. Saltzman and K. S. Schweizer, *Large-Amplitude Jumps and Non-Gaussian Dynamics in Highly Concentrated Hard Sphere Fluids*, Phys. Rev. E **77,** 051504 (2008).

[36] S. Mirigian and K. S. Schweizer, *Dynamical Theory of Segmental Relaxation and Emergent Elasticity in Supercooled Polymer Melts*, Macromolecules **48,** 1901 (2015).

[37] A. S. Keys, L. O. Hedges, J. P. Garrahan, S. C. Glotzer, and D. Chandler, *Excitations Are Localized and Relaxation Is Hierarchical in Glass-Forming Liquids*, Phys. Rev. X **1,** 021013 (2011).

[38] F. Ritort and P. Sollich, *Glassy Dynamics of Kinetically Constrained Models*, Adv. Phys. **52,** 219 (2003).

[39] R. G. Palmer, D. L. Stein, E. Abrahams, and P. W. Anderson, *Models of Hierarchically Constrained Dynamics for Glassy Relaxation*, Phys. Rev. Lett. **53,** 958 (1984).

[40] L.-N. Zou, X. Cheng, M. L. Rivers, H. M. Jaeger, and S. R. Nagel, *The Packing of Granular Polymer Chains*, Science **326,** 408 (2009).

[41] J. R. Fried, *Sub-T_g Transitions*, in *Physical Properties of Polymers Handbook* (Springer, New York, 2007), pp. 217–232.

[42] F. Kremer and A. Schönhals, *Broadband Dielectric Spectroscopy* (Springer Science & Business Media, New York, 2012).

[43] G. Smith and D. Bedrov, *Relationship between the α and β-Relaxation Processes in Amorphous Polymers: Insight from Atomistic Molecular Dynamics Simulations of 1,4-Polybutadiene Melts and Blends*, Polymer **45,** 627 (2007).

[44] R. Beevers and E. White, *Physical Properties of Vinyl Polymers. Part 1. Dependence of the Glass-Transition Temperature of Poly(methylmethacrylate) on Molecular Weight*, Trans. Faraday Soc. **56,** 744 (1960).

[45] V. Novikov and E. Rössler, *Correlation between Glass Transition Temperature and Molecular Mass in Non-polymeric and Polymer Glass Formers*, Polymer **54,** 6987 (2013).

[46] R. Boyer, *Variation of Polymer Glass Temperatures with Molecular Weight*, Macromolecules **7,** 142 (1974).

[47] J. M. G. Cowie and I. J. McEwen, *Molecular Motions in Poly(dimethyl siloxane) Oligomers and Polymers*, Polymer **14,** 423 (1973).

[48] The $T_g(M)$ data for n-alkanes (PE) were determined from viscosity measurements based on the definition $\log(\eta(T_g)) \equiv 13$ [49], which typically gives a different T_g than a definition based on a relaxation time $\tau_\alpha(T_g) \equiv 100$ s.

[49] A. Miller, *Kinetic Interpretation of the Glass Transition: Glass Temperatures of N-Alkane Liquids and Polyethylene*, J. Polym. Sci., A-2, Polym. Phys. **6,** 249 (1968).

[50] L. Fetters, D. Lohse, and R. Colby, *Chain Dimensions and Entanglement Spacings*, in *Physical Properties of Polymers Handbook* (Springer, New York, 2007), pp. 447–454.

[51] A. Agapov and A. P. Sokolov, *Size of the Dynamic Bead in Polymers*, Macromolecules **43,** 9126 (2010).

[52] Y. Ding and A. Sokolov, *Comment on the Dynamic Bead Size and Kuhn Segment Length in Polymers: Example of Polystyrene*, J. Polym. Sci., Part B: Polym. Phys. **42,** 3505 (2004).

[53] P. J. Flory, *Statistical Mechanics of Chain Molecules* (Carl Hansen Verlag, New York, 1989).

[54] H. Weyland, P. Hoftyzer, and D. V. Krevelen, *Prediction of the Glass Transition Temperature of Polymers*, Polymer **11,** 79 (1970).

[55] S. Matsuoka, *Entropy, Free Volume, and Cooperative Relaxation*, J. Res. Natl. Inst. Stand. Technol. **102,** 213 (1997).

[56] H. A. Schneider, *Polymer Class Specificity of the Glass Temperature*, Polymer **46,** 2230 (2005).

[57] J. Schut, D. Bolikal, I. Khan, A. Pesnell, A. Rege, R. Rojas, L. Sheihet, N. Murthy, and J. Kohn, *Glass Transition Temperature Prediction of Polymers through the Mass-per-Flexible-Bond Principle*, Polymer **48,** 6115 (2007).

[58] T. Kreer, J. Baschnagel, M. Müller, and K. Binder, *Monte Carlo Simulation of Long Chain Polymer Melts: Crossover from Rouse to Reptation Dynamics*, Macromolecules **34,** 1105 (2001).

[59] Y. Nakamura and T. Norisuye, *Polymer Properties in Solutions*, in *Polymer Science: A Comprehensive Reference*, edited by K. Matyjaszewski and M. Möller (Elsevier, New York, 2012).

[60] T. M. Birshtein, O. B. Ptitsyn, and E. A. Sokolova, *Internal Rotation in Polymer Chains and Their Physical Properties. XVII. Conformations of Polyisobutylene and Polydimethylsiloxane Molecules in Solution*, Vysokomolekul. Soedin. **1**, 852 (1959).

[61] The $T_g(M)$ for PDMS was previously compared to the jamming of granular bead chains, in which loops were proposed to control the packing [40].

[62] For PDMS, it was previously suggested that $T_g(M)$ behaves similarly to $C_n(M)$ [20,36,63]. In those studies, $C_n(M,T)$ was determined for a constant $T > T_g^\infty$, where the many gauche states inhibit loop formation, and thus the maximum of $C_n(M, T_g(M))$ for PDMS was not apparent.

[63] K. Chee, *Dependence of Glass Transition Temperature on Chain Flexibility and Intermolecular Interactions in Polymers*, J. Appl. Polym. Sci. **43**, 1205 (1991).

[64] A. Agapov and A. Sokolov, *Does the Molecular Weight Dependence of t_g Correlate to m_e?*, Macromolecules **42**, 2877 (2009).

[65] B. Schmidtke, N. Petzold, R. Kahlau, and E. Rössler, *Reorientational Dynamics in Molecular Liquids as Revealed by Dynamic Light Scattering: From Boiling Point to Glass Transition Temperature*, J. Chem. Phys. **139**, 084504 (2013).

[66] R. J. Larsen and C. F. Zukoski, *Effect of Particle Size on the Glass Transition*, Phys. Rev. E **83**, 051504 (2011).

[67] L. Zhang, J. A. Marsiglio, T. Lan, and J. M. Torkelson, *Dramatic Tunability of the Glass Transition Temperature and Fragility of Low Molecular Weight Polystyrene by Initiator Fragments Located at Chain Ends*, Macromolecules **49**, 2387 (2016).

[68] E. Hempel, G. Hempel, A. Hensel, C. Schick, and E. Donth, *Characteristic Length of Dynamic Glass Transition near T_g for a Wide Assortment of Glass-Forming Substances*, J. Phys. Chem. B **104**, 2460 (2000).

[69] W. Paul and G. Smith, *Structure and Dynamics of Amorphous Polymers: Computer Simulations Compared to Experiment and Theory*, Rep. Prog. Phys. **67** 1117 (2004).

[70] A. Arbe, U. Buchenau, L. Willner, D. Richter, B. Farago, and J. Colmenero, *Study of the Dynamic Structure Factor in the β Relaxation Regime of Polybutadiene*, Phys. Rev. Lett. **76**, 1872 (1996).

[71] A. Hofmann, A. Alegria, J. Colmenero, L. Willner, E. Buscaglia, and N. Hadjichristidis, *Secondary and Segmental Relaxation in Polybutadienes of Varying Microstructure: Dielectric Relaxation Results*, Macromolecules **29**, 129 (1996).

[72] R. D. Deegan and S. R. Nagel, *Dielectric Susceptibility Measurements of the Primary and Secondary Relaxation in Polybutadiene*, Phys. Rev. B **52**, 5653 (1995).

[73] D. Richter, R. Zorn, B. Farago, B. Frick, and L. Fetters, *Decoupling of Time Scales of Motion in Polybutadiene Close to the Glass Transition*, Phys. Rev. Lett. **68**, 71 (1992).

[74] T. Körber, F. Mohamed, M. Hofmann, A. Lichtinger, L. Willner, and E. A. Rössler, *The Nature of Secondary Relaxations: The Case of Poly(ethylene-alt-propylene) Studied by Dielectric and Deuteron NMR Spectroscopy*, Macromolecules **50**, 1554 (2017).

[75] S. Lusceac, C. Gainaru, M. Vogel, C. Koplin, P. Medick, and E. Rössler, *Secondary Relaxation Processes in Polybutadiene Studied by ^{2}H Nuclear Magnetic Resonance and High-Precision Dielectric Spectroscopy*, Macromolecules **38**, 5625 (2005).

[76] V. Bershtein, V. Egorov, L. Egorova, and V. Ryzhov, *The Role of Thermal Analysis in Revealing the Common Molecular Nature of Transitions in Polymers*, Thermochim. Acta **238**, 41 (1994).

[77] In this paper, we refer to the barrier that accompanies the α relaxation as an "enthalpic barrier," determined from matching the VFT fit of α-relaxation data to an Arrhenius form with a T-dependent enthalpy. Any entropic contributions to the barrier act as a prefactor to the exponential.

[78] R. Casalini and C. Roland, *Aging of a Low Molecular Weight Poly(methyl methacrylate)*, J. Non-Cryst. Solids **357**, 282 (2011).

[79] A. Kudlik, C. Tschirwitz, T. Blochowicz, S. Benkhof, and E. Rössler, *Slow Secondary Relaxation in Simple Glass Formers*, J. Non-Cryst. Solids **235**, 406 (1998).

[80] A. S. Keys, J. P. Garrahan, and D. Chandler, *Calorimetric Glass Transition Explained by Hierarchical Dynamic Facilitation*, Proc. Natl. Acad. Sci. U.S.A. **110**, 4482 (2013).

[81] P. Chleboun, A. Faggionato, and F. Martinelli, *Time Scale Separation in the Low Temperature East Model: Rigorous Results*, J. Stat. Mech. (2013) L04001.

[82] Our proposed 3D-facilitation mechanism, where the α relaxation arises from facilitation of β relaxations, should also apply to nonpolymeric glass formers. Recent computer simulation work used a swap Monte Carlo technique to reach temperatures closer to T_g in equilibrium than previously achieved and observed a so-called excess wing on the high-frequency side of the α relaxation [83]. This feature is often observed in molecular glass formers and is typically interpreted either as a secondary β relaxation in the vicinity of the α relaxation or as a generic feature of the α relaxation itself [84,85]. Interestingly, this study found direct evidence that the relaxation contribution within the "excess wing" generates the α relaxation through dynamic facilitation. This observation thus appears to be consistent with the general nature of our proposed picture. We also note that dynamic phase transitions with links to dynamic facilitation have recently been suggested in computer simulation studies to explain interfacial effects in thin polymer films [86].

[83] B. Guiselin, C. Scalliet, and L. Berthier, *Microscopic Origin of Excess Wings in Relaxation Spectra of Deeply Supercooled Liquids*, Nat. Phys. **18**, 468 (2022).

[84] P. Lunkenheimer, U. Schneider, R. Brand, and A. Loidl, *Glassy Dynamics*, Contemp. Phys. **41**, 15 (2000).

[85] J. Mattsson, R. Bergman, P. Jacobsson, and L. Börjesson, *Chain-Length-Dependent Relaxation Scenarios in an Oligomeric Glass-Forming System: From Merged to*

Well-Separated α and β Loss Peaks, Phys. Rev. Lett. **90**, 075702 (2003).

[86] R. Ivancic and R. Riggleman, *Dynamic Phase Transitions in Freestanding Polymer Thin Films*, Proc. Natl. Acad. Sci. U.S.A. **117**, 25407 (2020).

[87] We note that the intramolecular facilitated relaxation mechanism suggested here could provide a much sought-for mechanism to explain dramatic effects on T_g with film thickness (and M) in thin polymer films, as observed for both PS and PMMA [88,89].

[88] J. A. Forrest and K. Dalnoki-Veress, *The Glass Transition in Thin Polymer Films*, Adv. Colloid Interface Sci. **94**, 167 (2001).

[89] S. Napolitano, E. Glynos, and N. Tito, *Glass Transition in Polymers in Bulk, Confined Geometries, and Near Interfaces*, Rep. Prog. Phys. **80**, 036602 (2017).

[90] L. J. Fetters, D. J. Lohse, S. T. Milner, and W. W. Graessley, *Packing Length Influence in Linear Polymer Melts on the Entanglement, Critical, and Reptation Molecular Weights*, Macromolecules **32**, 6847 (1999).

[91] P. Sollich and M. R. Evans, *Glassy Time-Scale Divergence and Anomalous Coarsening in a Kinetically Constrained Spin Chain*, Phys. Rev. Lett. **83**, 3238 (1999).

[92] The data in this paper are available in the Leeds Data Repository, at 10.5518/827.

[93] M. Rubinstein and R. H. Colby, *Polymer Physics* (Oxford University Press, New York, 2003), Vol. 23.

[94] M. Rehahn, W. L. Mattice, and U. W. Suter, *Rotational Isomeric State Models in Macromolecular Systems* (Springer, Berlin, Heidelberg, 1997).

[95] A. Boothroyd, A. Rennie, and G. Wignall, *Temperature Coefficients for the Chain Dimensions of Polystyrene and Poly(methylmethacrylate)*, J. Chem. Phys. **99**, 9135 (1993).

[96] R. Krishnamoorti, W. W. Graessley, A. Zirkel, D. Richter, N. Hadjichristidis, L. J. Fetters, and D. J. Lohse, *Melt-State Polymer Chain Dimensions as a Function of Temperature*, J. Polym. Sci., Part B: Polym. Phys. **40**, 1768 (2002).

[97] C. Hoeve, *Unperturbed Mean-Square End-to-End Distance of Polyethylene*, J. Chem. Phys. **35**, 1266 (1961).

[98] P. Flory, V. Crescenzi, and J. Mark, *Configuration of the Poly-(dimethylsiloxane) Chain. III. Correlation of Theory and Experiment*, J. Am. Chem. Soc. **86**, 146 (1964).

[99] D. Yoon, P. Sundararajan, and P. Flory, *Conformational Characteristics of Polystyrene*, Macromolecules **8**, 776 (1975).

[100] P. Sundararajan and P. Flory, *Configurational Characteristics of Poly(methyl methacrylate)*, J. Am. Chem. Soc. **96**, 5025 (1974).

[101] A. Abe, T. Hirano, and T. Tsuruta, *Conformational Energies and the Random-Coil Configuration of Poly(oxypropylene)*, Macromolecules **12**, 1092 (1979).

[102] S. S. Batsanov, *Van der Waals Radii of Elements*, Inorg. Mater. **37**, 871 (2001).

[103] H. Janszen, T. Tervoort, and P. Cifra, *Bimodality in the Spatial Segment Density Distribution of Gaussian Chains*, Macromolecules **29**, 5678 (1996).

[104] H. Yamakawa, *Modern Theory of Polymer Solutions* (Harper & Row, New York, 1971).

[105] L. Fetters, D. Lohse, D. Richter, T. Witten, and A. Zirkel, *Connection between Polymer Molecular Weight, Density, Chain Dimensions, and Melt Viscoelastic Properties*, Macromolecules **27**, 4639 (1994).

[106] J. Baschnagel, K. Qin, W. Paul, and K. Binder, *Monte Carlo Simulation of Models for Single Polyethylene Coils*, Macromolecules **25**, 3117 (1992).

[107] E. V. Thompson, *Dependence of the Glass Transition Temperature of Poly(methyl methacrylate) on Tacticity and Molecular Weight*, J. Polym. Sci., A-2, Polym. Phys. **4**, 199 (1966).

[108] K. O'Driscoll and R. A. Sanayei, *Chain-Length Dependence of the Glass Transition Temperature*, Macromolecules **24**, 4479 (1991).

[109] G. Bartenev and S. Y. Frenkel, *Polymer Physics* (Khimiya, Leningrad, 1990).

[110] P. Santangelo and C. Roland, *Molecular Weight Dependence of Fragility in Polystyrene*, Macromolecules **31**, 4581 (1998).

[111] K. Kirst, F. Kremer, T. Pakula, and J. Hollingshurst, *Molecular Dynamics of Cyclic and Linear Poly(dimethylsiloxanes)*, Colloid Polym. Sci. **272**, 1420 (1994).

[112] J. Sacristan, C. Chen, and J. K. Maranas, *Role of Effective Composition on Dynamics of PEO-PMMA Blends*, Macromolecules **41**, 5466 (2008).

[113] T. Tadano, R. Zhu, Y. Muroga, T. Hoshi, D. Sasaki, S. Yano, and T. Sawaguchi, *A New Mechanism for the Silica Nanoparticle Dispersion–Agglomeration Transition in a Poly(methyl methacrylate)/Silica Hybrid Suspension*, Polym. J. **46**, 342 (2014).

[114] G. Bartenev, N. Shut, S. Baglyuk, and V. Rupyshev, *Relaxational Transitions in Polystyrene and Their Classification*, Polym. Sci. USSR **30**, 2448 (1988).

[115] J. Roovers, R. Ethier, and P. Toporowski, *The Properties of 'RADEL R' Polysulfone*, High Perform. Polym. **2**, 151 (1990).

[116] Z. Dobkowski, *Influence of Molecular Weight Distribution and Long Chain Branching on the Glass Transition Temperature of Polycarbonate*, Eur. Polym. J. **18**, 563 (1982).

[117] K. Palczynski, A. Wilke, M. Paeschke, and J. Dzubiella, *Molecular Modeling of Polycarbonate Materials: Glass Transition and Mechanical Properties*, Phys. Rev. Mater. **1**, 043804 (2017).

[118] A. Abou Elfadl, R. Kahlau, A. Herrmann, V. Novikov, and E. Rössler, *From Rouse to Fully Established Entanglement Dynamics: A Study of Polyisoprene by Dielectric Spectroscopy*, Macromolecules **43**, 3340 (2010).

[119] A. R. Greenberg and R. P. Kusy, *Evaluation of the Gibbs-DiMarzio Theory for the Case of Polyisobutylene*, J. Polym. Sci., Part B: Polym. Phys. **25**, 435 (1987).

[120] R. H. Colby, L. J. Fetters, and W. W. Graessley, *The Melt Viscosity-Molecular Weight Relationship for Linear Polymers*, Macromolecules **20**, 2226 (1987).

[121] J. Mattsson, R. Bergman, P. Jacobsson, and L. Börjesson, *Influence of Chain Length on the α − β Bifurcation in Oligomeric Glass Formers*, Phys. Rev. Lett. **94**, 165701 (2005).

[122] R. Bergman, C. Svanberg, D. Andersson, A. Brodin, and L. Torell, *Relaxational and Vibrational Dynamics of*

Poly(propylene glycol), J. Non-Cryst. Solids **235**–**237**, 225 (1998).

[123] T. Alper, J. Barlow, and R. Walter Gray, *Comparison of the Dielectric and Viscoelastic Properties of Two Poly(propylene glycol) Liquids*, Polymer **17**, 665 (1976).

[124] T. Inoue and K. Osaki, *Role of Polymer Chain Flexibility on the Viscoelasticity of Amorphous Polymers around the Glass Transition Zone*, Macromolecules **29**, 1595 (1996).

[125] M. Hofmann, A. Herrmann, A. Abou Elfadl, D. Kruk, M. Wohlfahrt, and E. Rössler, *Glassy, Rouse, and Entanglement Dynamics as Revealed by Field Cycling* 1H *NMR Relaxometry*, Macromolecules **45**, 2390 (2012).

[126] M. Brereton, I. Ward, N. Boden, and P. Wright, *Nature of the Proton NM Transverse Relaxation Function of Polyethylene Melts. 1. Monodispersed Polyethylenes*, Macromolecules **24**, 2068 (1991).

[127] W. Graessley and S. Edwards, *Entanglement Interactions in Polymers and the Chain Contour Concentration*, Polymer **22**, 1329 (1981).

[128] B. A. Smith, E. T. Samulski, L. P. Yu, and M. A. Winnik, *Polymer Diffusion in Molten Poly(propylene oxide)*, Macromolecules **18**, 1901 (1985).

[129] C. Gainaru, W. Hiller, and R. Bohmer, *A Dielectric Study of Oligo- and Poly(propylene glycol)*, Macromolecules **43**, 1907 (2010).

[130] S. Wu, *Chain Structure and Entanglement*, J. Polym. Sci., Part B: Polym. Phys. **27**, 723 (1989).

[131] D. W. Van Krevelen and K. T. Nijenhuis, *Properties of Polymers: Their Correlation with Chemical Structure; Their Numerical Estimation and Prediction from Additive Group Contributions*, 4th ed. (Elsevier, Amsterdam, 2009).

[132] J. Cowie, *Glass Transition Temperatures of Stereoblock, Isotactic and Atactic Polypropylenes of Various Chain Lengths*, Eur. Polym. J. **9**, 1041 (1973).

[133] S. Shenogin, R. Kant, R. H. Colby, and S. K. Kumar, *Dynamics of Miscible Polymer Blends: Predicting the Dielectric Response*, Macromolecules **40**, 5767 (2007).

[134] J. G. Ribelles, R. Diaz-Calleja, R. Ferguson, and J. Cowie, *Glass Transition and Physical Ageing in Plasticized Poly(vinyl chloride)*, Polymer **28**, 2262 (1987).

[135] Y. Zhang, J. Zhang, Y. Lu, Y. Duan, S. Yan, and D. Shen, *Glass Transition Temperature Determination of Poly(ethylene terephthalate) Thin Films Using Reflection-Absorption FTIR*, Macromolecules **37**, 2532 (2004).

[136] N. G. McCrum, B. E. Read, and G. Williams, *Anelastic and Dielectric Effects in Polymeric Solids* (Wiley, New York, 1967).

[137] L. D'ilario, M. Lucarini, A. Martinelli, and A. Piozzi, *Poly(p-phenylene sulfide) Glass Transition Temperature Evidenced by IR Spectroscopy*, Eur. Polym. J. **33**, 1809 (1997).

[138] J. Sandler, P. Werner, M. S. Shaffer, V. Demchuk, V. Altstädt, and A. H. Windle, *Carbon-Nanofibre-Reinforced Poly(ether ether ketone) Composites*, Composites, Part A **33**, 1033 (2002).

[139] P. Törmälä, *Determination of Glass Transition Temperature of Poly(ethylene glycol) by Spin Probe Technique*, Eur. Polym. J. **10**, 519 (1974).

[140] M. Varma-Nair, J. Cheng, Y. Jin, and B. Wunderlich, *Thermal Properties of Polysilylenes*, Macromolecules **24**, 5442 (1991).

[141] M. Fujino, T. Hisaki, M. Fujiki, and N. Matsumoto, *Preparation and Characterization of a Novel Organopolysilane. (3, 3, 3-trifluoropropyl) Methylpolysilane*, Macromolecules **25**, 1079 (1992).

[142] J. Fonseca, C. Barker, and J. Badyal, *Plasma Oxidation of Poly(cyclohexylmethylsilane) and Poly(phenylmethylsilane) Thin Films*, Macromolecules **28**, 6112 (1995).

[143] A. Sengupta and M. Fayer, *Ultrafast Nonexponential Dynamics in a Polymer Glass Forming Liquid*, J. Chem. Phys. **100**, 1673 (1994).

[144] V. Novikov and E. Rössler, *Correlation between Glass Transition Temperature and Molecular Mass in Nonpolymeric and Polymer Glass Formers*, Polymer **54**, 6987 (2013).

[145] J. Roovers, P. Toporowski, and R. Ethier, *Viscoelastic Properties of Melts of 'RADEL-R' Polysulphone Fractions*, High Performance Polymers **2**, 165 (1990).

[146] J. Fried, A. Letton, and W. Welsh, *Secondary Relaxation Process in Bisphenol-A Polysulphone*, Polymer **31**, 1032 (1990).

[147] J. Crissman, A. Woodward, and J. Sauer, *Dynamic Mechanical Behavior of Polystyrene and Related Polymers at Temperatures from* 4.2 °K, J. Polym. Sci., Part A: Gen. Pap. **3**, 2693 (1965).

[148] A. Alegria, S. Arrese-Igor, O. Mitxelena, and J. Colmenero, *Dielectric Secondary Relaxation and Phenylene Ring Dynamics in Bisphenol-A Polycarbonate*, J. Non-Cryst. Solids **353**, 4262 (2007).

[149] A. Alegria, O. Mitxelena, and J. Colmenero, *On the Molecular Motions Originating from the Dielectric γ-Relaxation of Bisphenol-A Polycarbonate*, Macromolecules **39**, 2691 (2006).

[150] J. Jho and A. Yee, *Secondary Relaxation Motion in Bisphenol A Polycarbonate*, Macromolecules **24**, 1905 (1991).

[151] K. Schmidt-Rohr, A. Kulik, H. Beckham, A. Ohlemacher, U. Pawlzik, C. Boeffel, and H. Spiess, *Molecular Nature of the β Relaxation in Poly(methyl methacrylate) Investigated by Multidimensional NMR*, Macromolecules **27**, 4733 (1994).

[152] S. Kuebler, D. Schaefer, C. Boeffel, U. Pawelzik, and H. Spiess, *2D Exchange NMR Investigation of the α-Relaxation in Poly(ethyl methacrylate) as Compared to Poly(methyl methacrylate)*, Macromolecules **30**, 6597 (1997).

[153] S. Arrese-Igor, A. Arbe, B. Frick, and J. Colmenero, *Glassy Dynamics of Polystyrene by Quasielastic Neutron Scattering*, Macromolecules **44**, 3161 (2011).

[154] S. Kolodziej, S. Pawlus, K. Ngai, and M. Paluch, *Verifying the Approximate Coinvariance of the α and Johari-Goldstein β Relaxation Times to Variations of Pressure and Temperature in Polyisoprene*, Macromolecules **51**, 4435 (2018).

[155] C. Roland, M. Schroeder, J. Fontanella, and K. Ngai, *Evolution of the Dynamics in 1,4-Polyisoprene from a Nearly Constant Loss to a Johari-Goldstein β-Relaxation to the α-Relaxation*, Macromolecules **37**, 2630 (2004).

[156] A. Arbe, J. Colmenero, B. Frick, M. Monkenbusch, and D. Richter, *Investigation of the Dielectric β-Process in Polyisobutylene by Incoherent Quasielastic Neutron Scattering*, Macromolecules **31**, 4926 (1998).

[157] J. Mattsson, R. Bergman, P. Jacobsson, and L. Börjesson, *Effects of Hydrogen Bonding on Supercooled Liquid Dynamics and the Implications for Supercooled Water*, Phys. Rev. B **79**, 174205 (2009).

[158] R. Boyd and S. Breitling, *The Conformational Analysis of Crankshaft Motions in Polyethylene*, Macromolecules **7**, 855 (1974).

[159] T. Atvars, E. Sabadini, and S. Martins-Franchetti, *Study of the Secondary Relaxations of Polyethylene by Photoluminescence Techniques*, Polymer **29**, 1259 (1993).

[160] R. Caslini, K. Ngai, C. Robertson, and C. Roland, *α and β-Relaxations in Neat and Antiplasticized Polybutadiene*, J. Polym. Sci., Part B: Polym. Phys. **38**, 1841 (2000).

[161] D. Bedrov and G. Smith, *Molecular Dynamics Simulation Study of the α and β-Relaxation Processes in a Realistic Model Polymer*, Phys. Rev. E **71**, 050801(R) (2005).